研究成果の刊行に関する一覧表

書籍

著者氏名	論文タイトル名	書籍全体の編集者名	書　籍　名	出版社名	出版地	出版年	ページ
川﨑俊之、田原強、宿里充穂、尾上浩隆	再生医療への分子イメージングの応用	佐治英郎	遺伝子医学MOOK18 創薬研究への分子イメージング応用	株式会社メディカル ドゥ	大阪	2010	206-213
尾上浩隆、川崎俊之	PET分子イメージングと再生医療	米倉義晴、伊藤雅敏、窪田和雄、佐治英郎、玉木長良、中川恵一、畑澤順、間賀田泰寛、渡辺恭良、寺田弘司	先端医療シリーズ14 臨床医とコメディカルのための最新クリニカルPET	株式会社寺田国際事務所/先端医療技術研究所	東京	2010	292-296

雑誌

発表者氏名	論文タイトル名	発表誌名	巻号	ページ	出版年
Takashima-Hirano M, Shukuri M, Takashima T, Goto M, Wada Y, Watanabe Y, Onoe H, Doi H, Suzuki M.	General Method for the (11)C-Labeling of 2-Arylpropionic Acids and Their Esters: Construction of a PET Tracer Library for a Study of Biological Events Involved in COXs Expression.	Chemistry	16(14)	4250-4258	2010
Kikuchi T., Morizane A., Doi D., Onoe H., Hayashi T., Kawasaki T., Saiki H., Miyamoto S., Takahashi J.	Dopaminergic neurons generated from human induced pluripotent stem cells in a primate model of Parkinson's disease.	Journal of Parkinson's Disease	1(4)	395-412	2011
高橋　淳、尾上浩隆	再生医療における分子イメージング	JSMI Report	5(1)	3-5	2012
Doi D., Morizane A., Kikuchi T., Onoe H., Hayashi T., Kawasaki T., Motono M., Sasai Y., Saiki H., Gomi M., Yoshikawa T., Hayashi H., Shinoyama M., Mohamed R., Suemori H., Miyamoto S., Takahashi J.	Prolonged Maturation Culture Favors a Reduction in the Tumorigenicity and the Dopaminergic Function of Human ESC-Derived Neural Cells in a Primate Model of Parkinson's Disease.	Stem Cells		*in press*	2012

III. 研究成果の刊行物・別冊

CHEMISTRY
A EUROPEAN JOURNAL

DOI: 10.1002/chem.200903044

General Method for the ^{11}C-Labeling of 2-Arylpropionic Acids and Their Esters: Construction of a PET Tracer Library for a Study of Biological Events Involved in COXs Expression

Misato Takashima-Hirano, Miho Shukuri, Tadayuki Takashima, Miki Goto, Yasuhiro Wada, Yasuyoshi Watanabe, Hirotaka Onoe, Hisashi Doi, and Masaaki Suzuki*[a]

Abstract: Cyclooxygenase (COX) is a critical enzyme in prostaglandin biosynthesis that modulates a wide range of biological functions, such as pain, fever, and so on. To perform in vivo COX imaging by positron emission tomography (PET), we developed a method to incorporate ^{11}C radionuclide into various 2-arylpropionic acids that have a common methylated structure, particularly among nonsteroidal anti-inflammatory drugs (NSAIDs). Thus, we developed a novel ^{11}C-radiolabeling methodology based on rapid *C*-[^{11}C]methylation by the reaction of [^{11}C]CH_3I with enolate intermediates generated from the corresponding esters under basic conditions. One-pot hydrolysis of the above [^{11}C]methylation products also allows the synthesis of desired ^{11}C-incorporated acids. We demonstrated the utility of this method in the syntheses of six PET tracers, [^{11}C]Ibuprofen, [^{11}C]Naproxen, [^{11}C]Flurbiprofen, [^{11}C]Fenoprofen, [^{11}C]Ketoprofen, and [^{11}C]Loxoprofen. Notably, we found that their methyl esters were particularly useful as proradiotracers for a study of neuroinflammation. The microPET studies of rats with lipopolysaccharide (LPS)-induced brain inflammation clearly showed that the radioactivity of PET tracers accumulated in the inflamed region. Among these PET tracers, the specificity of [^{11}C]Ketoprofen methyl ester was demonstrated by a blocking study. Metabolite analysis in the rat brain revealed that the methyl esters were initially taken up in the brain and then underwent hydrolysis to form pharmacologically active forms of the corresponding acids. Thus, we succeeded in general ^{11}C-labeling of 2-arylpropionic acids and their methyl esters as PET tracers of NSAIDs to construct a potentially useful PET tracer library for in vivo imaging of inflammation involved in COXs expression.

Keywords: anti-inflammatory drugs · C–C coupling · cyclooxygenase · inflammation · positron emission tomography

Introduction

Nonsteroidal anti-inflammatory drugs (NSAIDs) are among the most widely prescribed drugs worldwide, because they are the first choice in the treatment of rheumatic disorders and other degenerative inflammatory diseases.[1] One of the pharmacological actions of NSAIDs is an inhibitory effect on cyclooxygenase (COX), which is a critical enzyme in converting arachidonic acid into prostaglandins and thromboxanes. Mainly, two distinct isoforms, COX-1 and COX-2, are known as a constitutive and an inducible form, respectively. Recently, a novel COX-1 splice variant termed as COX-3 has also been reported.[2] COX-1 enzyme exists in most mammalian cells including the endothelium, stomach, and kidney, and is responsible for maintaining homeostasis. In contrast, COX-2 is found in the brain and kidney, it is primarily induced in response to cytokines, mitogens, and endotoxins in a variety of cell types including macrophages and tumors. Therefore, the quantification of COX-2 in many disease processes has great potential as a useful biomarker for early diagnosis, a monitor of disease progression, and an indicator of effective medical treatment.

[a] M. Takashima-Hirano, M. Shukuri, T. Takashima, M. Goto, Y. Wada, Prof. Dr. Y. Watanabe, Dr. H. Onoe, Dr. H. Doi, Prof. Dr. M. Suzuki
RIKEN Center for Molecular Imaging Science (CMIS)
6-7-3 Minatojima-minamimachi, Chuo-ku
Kobe, Hyogo, 650-0047 (Japan)
Fax: (+81) 78-304-7131
E-mail: masaaki.suzuki@riken.jp

Supporting information for this article is available on the WWW under http://dx.doi.org/10.1002/chem.200903044.

Positron emission tomography (PET) is a powerful noninvasive molecular imaging technique that provides high sensitivity, good spatial resolution, and easy and accurate quantification; PET is frequently used in biological research and clinical studies.[3] Radionuclides used in PET include short-lived radioisotopes (^{11}C, ^{13}N, ^{15}O) of the abundant elements in the structures of biologically active compounds, such as natural products and drugs, etc. A dose of the labeled compound in medicine is very tiny, namely less than 1/100 of actual pharmacological dose or 100 μg.[4] Therefore, the application of PET in a human microdose study at an early stage of drug and biomarker development has been expected.[5] The increasing need for pharmacologically significant PET tracers requires efficient synthetic strategies for new molecular tracer designs and advances in radiolabeling methodology. Carbon-11 (half-life = 20.4 min) is one of the most important isotopes for PET research. In particular, the incorporation of the [^{11}C]methyl group into organic frameworks through [^{11}C]carbon–carbon bond formation is one of the attractive approaches because 1) the [^{11}C]methyl group can be introduced into a metabolically stable position in the molecules and, therefore, such a ^{11}C-labeled tracer provides a highly credible PET image, 2) the methyl group is often used in drug design to control the lipophilicity of the molecule and the blocking of the metabolic position as the smallest substituted group containing carbon, and 3) the short half-life of the ^{11}C-incorporated tracer allows rapid screening of the PET images and increases progress by several trials per day.[6]

Since the discovery of COX-2, the development of drugs that selectively inhibit this isoform and the development of corresponding specific PET tracers have become a major area of pharmaceutical research.[7] During the past decade, PET tracers corresponding to highly selective and potent COX-2 inhibitors, such as [^{18}F]desbromo-Dup-697,[8] [^{11}C]Celecoxib,[9] [^{11}C]Rofecoxib,[10] and [^{11}C]Valdecoxib[11] have been developed. Additionally, ^{11}C-labeling of diaryl-substituted imidazole and indole analogues has yielded PET probes with a high affinity and selectivity for COX-2.[12] However, to the best of our knowledge, the successful COX-2 imaging by using these PET tracers has not yet been reported.[13]

The cause of the adverse side effects of NSAIDs is suspected to be the inhibition of COX-1, a necessary housekeeping gene that is not elevated during inflammation. In contrast, COX-2 is normally nondetectable in most tissues, but is rapidly elevated during inflammation. Thus, the inhibition of COX-2 by NSAIDs is thought to be responsible for their therapeutic effects. However, the relative biological contributions of COX-1 and COX-2 isoforms in the maintenance of normal physiological functions and in disease states are not entirely clear.[14] Therefore, the development of both nonselective and selective COX inhibitors and the evaluation of their in vivo behavior by PET imaging could greatly help to elucidate their physiological actions.

We previously developed a simple method to synthesize [^{11}C]Celecoxib, a COX-2 inhibitor.[15] In the present report, we describe the efficient general syntheses of ^{11}C-labeled 2-arylpropionic esters by rapid [^{11}C]methylation through sp^3–sp^3-type coupling by the reaction of [^{11}C]CH_3I and the corresponding enolates with the aim of realizing COX imaging by PET. These esters were readily converted to the corresponding acids as NSAID structures by one-pot hydrolysis.[16] The evaluation of the blood-brain barrier (BBB) permeability of these NSAIDs PET tracers in rats and in vivo studies of a rat lipopolysaccharide (LPS)-induced inflammation model are also described.

Results and Discussions

Chemistry: The 2-arylpropionic acids of six NSAIDs, Ibuprofen, Naproxen, Flurbiprofen, Fenoprofen, Ketoprofen, and Loxoprofen, were selected for ^{11}C-labeling. They share a common chemical structure for [^{11}C]methyl group introduction, despite their different levels of inhibition of COX-1 and COX-2.[17] All precursors and authentic samples were prepared according to conventional synthetic methods or purchased as described in the Experimental Section.[18]

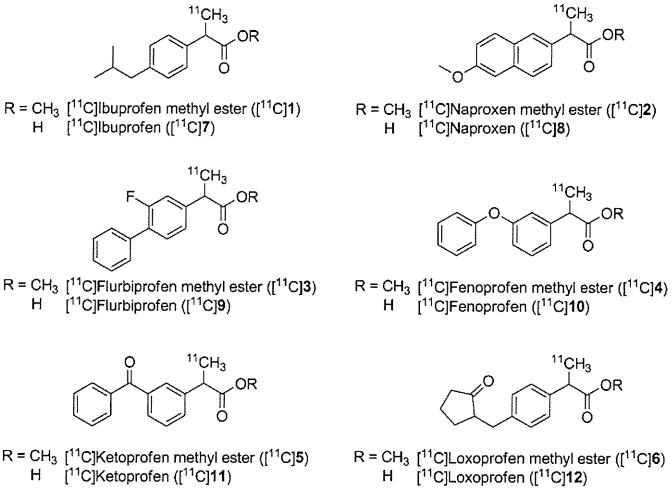

Radiochemistry: Scheme 1 illustrates the syntheses of ^{11}C-labeled 2-arylpropionic acids and their esters; the syntheses were based on rapid *C*-[^{11}C]methylation by using [^{11}C]CH_3I under basic conditions. In general, sodium hydride was added to a solution of methyl arylacetate as a precursor in

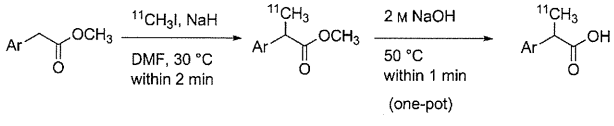

Scheme 1. Syntheses of ^{11}C-labeled 2-arylpropionic acids and their methyl esters.

DMF at room temperature for the deprotonation of the benzylic position. After 10–20 min, [^{11}C]CH_3I with He flow (30 mL min^{-1}) was trapped in the mixture and reacted with the enolate at 30 °C for 2 min, and then the resulting mixture was quickly subjected to the preparative HPLC operation because of the rapid completion of the *C*-[^{11}C]methylation. When the reaction was continued for a slightly longer time or at a slightly higher temperature after [^{11}C]CH_3I trapping, the yield of the [^{11}C]methylated compounds was decreased. In the synthesis of [^{11}C]Ketoprofen methyl ester ([^{11}C]**5**), when the reaction mixture was heated at 50 °C or left for several minutes after [^{11}C]CH_3I trapping, the desired product [^{11}C]**5** was gradually decomposed with time, and some unknown side products appeared (Figure 1).

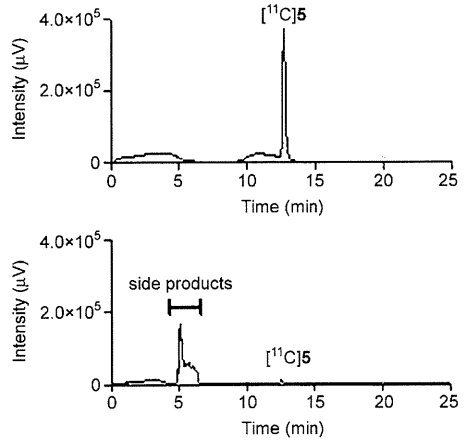

Figure 1. Radiochromatograms of the crude reaction mixture of [^{11}C]Ketoprofen methyl ester ([^{11}C]**5**) obtained by the reaction of [^{11}C]CH_3I and methyl (3-benzoylphenyl)acetate, demethylated precursor. A) [^{11}C]CH_3I trapping at 30 °C for 2 min. B) [^{11}C]CH_3I trapping at 30 °C for 2 min and reaction at 50 °C for 4 min.

Finally, [^{11}C]**5** was almost completely decomposed after the reaction for 4 min at 50 °C (Figure 1B). After extensive experiments, we found that the reaction was completed during [^{11}C]CH_3I trapping at 30 °C without further reaction time. This reaction was also proceeded by [^{11}C]CH_3I trapping at −10 °C. By using these conditions, [^{11}C]Ibuprofen methyl ester ([^{11}C]**1**), [^{11}C]Naproxen methyl ester ([^{11}C]**2**), [^{11}C]Flurbiprofen methyl ester ([^{11}C]**3**), [^{11}C]Fenoprofen methyl ester ([^{11}C]**4**), and [^{11}C]Loxoprofen methyl ester ([^{11}C]**6**) were efficiently synthesized. Inexplicably, the compounds, [^{11}C]**1**, [^{11}C]**2**, [^{11}C]**5**, and [^{11}C]**6** tended to decompose upon radiolyses. In particular, [^{11}C]**1** and [^{11}C]**2** were gradually decomposed during HPLC purification or concentration by evaporator. However, in our experience, we have found that such radiolyses could be prevented by the use of [^{11}C]CH_3I at less than 15 GBq. The addition of ascorbic acid as an antioxidant stabilizer to the reaction mixture before the HPLC purification also effectively prevented the radiolysis.[19] Consequently, we found that the six kinds of 2-aryl-[^{11}C]propionic acid methyl esters are stable for 2 h after purification by analytical HPLC. At present, the mechanism of the radiolytic decomposition and the intrinsic stability of the methyl esters are not clear. In addition, the corresponding carboxylic acids, [^{11}C]Ibuprofen ([^{11}C]**7**), [^{11}C]Naproxen ([^{11}C]**8**), [^{11}C]Flurbiprofen ([^{11}C]**9**), [^{11}C]Fenoprofen ([^{11}C]**10**), [^{11}C]Ketoprofen ([^{11}C]**11**), and [^{11}C]Loxoprofen ([^{11}C]**12**), were also synthesized in one-pot reactions by the rapid hydrolysis of each 2-aryl[^{11}C]propionic acid methyl ester with 2 M sodium hydroxide at 50 °C for 1 min. This hydrolysis completed even at 30 °C for 1 min. Interestingly, ^{11}C-labeled 2-arylpropionic acids were radiochemically stable. The physicochemical properties of the labeled compounds are listed in Table 1. All 12 ^{11}C-labeled compounds

Table 1. Synthetic results and the stability of ^{11}C-labeled 2-arylopropionic acids and their methyl esters.

Compound	Radioactivity [GBq][a]	Specific radioactivity [GBq μmol^{-1}]	DCY [%]	Stability[b]
methyl ester				
[^{11}C]**1**	3.1±0.8	20±2.9	56±17	C
[^{11}C]**2**	2.4±0.1	32±7.6	48±5.7	C
[^{11}C]**3**	5.5±0.2	40±1.5	76±12	A
[^{11}C]**4**	2.9±1.9	38±5.6	43±24	A
[^{11}C]**5**	5.5±0.4	47±11	72±13	B
[^{11}C]**6**	1.9±0.1	26±8.7	26±5.3	B
carboxylic acid				
[^{11}C]**7**	4.3±0.7	25±8.5	72±15	A
[^{11}C]**8**	2.7±0.6	24±1.0	47±12	A
[^{11}C]**9**	2.8±0.3	31±12	43±6.7	A
[^{11}C]**10**	3.3±2.3	20±5.0	60±21	A
[^{11}C]**11**	3.0±0.6	30±15	29±13	A
[^{11}C]**12**	1.6±0.6	22±6.9	29±13	A

Data are expressed as mean ±SD ([^{11}C]**1**, [^{11}C]**2**, [^{11}C]**3**, [^{11}C]**4**, [^{11}C]**7**, [^{11}C]**9**, [^{11}C]**10**, [^{11}C]**11**, and [^{11}C]**12**, $n=3$; [^{11}C]**5**, [^{11}C]**6**, and [^{11}C]**8**, $n=4$). [a] Radioactivity showing the isolated radioactivity. [b] A: stable, B: stable in the presence of ascorbic acid, C: stable under the lower current beam and in the presence of ascorbic acid; DCY: decay-corrected yield based on [^{11}C]CH_3I.

that we synthesized by the above procedures possessed sufficient radioactivity (1.7–5.5 GBq) for an animal PET study. The decay-corrected radiochemical yields (DCY) based on [^{11}C]CH_3I were 26–76%. Of these, the yields of [^{11}C]**12** and its methyl ester [^{11}C]**6** were relatively low. Such low yields were presumably due to the co-occurrence of the enolization at both of the α-positions of the ester and ketone moieties. We classified isolated [^{11}C] products into three groups based on their radiochemical stability. [^{11}C]**3**, [^{11}C]**4**, [^{11}C]**7**, [^{11}C]**8**, [^{11}C]**9**, [^{11}C]**10**, [^{11}C]**11**, and [^{11}C]**12** were stably isolated without the addition of ascorbic acid, and they were categorized as class A. [^{11}C]**5** and [^{11}C]**6** in class B required ascorbic acid for the HPLC purification and evaporation. [^{11}C]**1** and [^{11}C]**2** in class C were very unstable, and they required not only ascorbic acid but also synthetic conditions with the lower radioactivity (~15 GBq). The reaction with higher radioactivity (>15 GBq) gave many kinds of products among which it was too difficult to isolate the desired labeled compound. The chemical and radiochemical purities of the isolated products were greater than 98% because of their un-

expectedly ready separation from their corresponding demethylated precursors.[20] Here, we consider that such a large polarity difference between methylated and demethylated compounds, as indicated in reverse-phase HPLC, may be caused by the following electronic and structural factors: The first factor is the ordinary increase of hydrophobicity by introducing a nonpolar methyl group into an organic framework. The second factor is the decrease of the acidity of the benzylic proton of methylated compounds that is attributed to the hyperconjugation between the C–H σ bond of a benzylic position and C=O π*, which is also possible for the LUMO (π*) of a phenyl moiety. Such hyperconjugation in methylated products, if any, would also be less favored in the methylated compound because of steric congestion emerging from the assumed fully substituted pseudo olefin structure.

Brain penetration of [^{11}C]5 and [^{11}C]11 evaluated by microPET imaging: PET scans were performed to measure the uptake of [^{11}C]**5** and [^{11}C]**11** in the inflamed area of the left striatum in rats; the inflammation was induced by the injection of 50 μg of lipopolysaccharide (LPS) one day before the PET scan, because it was reported to cause the activation of microglia within 24 h.[21] In this condition, we have also observed the increase of the COX-2 expression surrounding the LPS injection site by the immunohistochemical method (data not shown). Radioactivity of [^{11}C]**5** after intravenous bolus administration was highly accumulated into the LPS injection site and the surrounding area, whereas radioactivity of [^{11}C]**11** after the administration was not accumulated in the brain including the injected site (Figure 2). The radioactivity of [^{11}C]**5** in the inflammatory area was about 9-fold higher than that of [^{11}C]**11**. Low penetration of [^{11}C]**11** into the brain, which was consistent with a previous study that used 2-arylpropionic acids,[22] was dramatically improved by the conversion of carboxylic acid into methyl ester.[23] As compared with [^{11}C]PK11195, which is one of the PET tracers widely used for the imaging of activated microglia that have occurred by neuroinflammation, the SUV level of [^{11}C]**5** in the brain is almost the same, and moreover, the ratio of radioactivity in the inflammatory region to background is rather superior.[24] Therefore, [^{11}C]**5** could be applicable for the PET imaging of neuroinflammation.

Measurement of [^{11}C]5 and the radioactive metabolites in rat brain and blood: Metabolite analyses in rat brain and blood of the ester as proradiotracers were performed in normal rats after the administration of [^{11}C]**5** (Figure 3). [^{11}C]**5** was rapidly hydrolyzed in rat blood to the pharmacologically active form [^{11}C]**11**, and the hydrolysis rate of [^{11}C]**5** in rat brain was much slower than that in the blood. Thus more than 90% of [^{11}C]**5** that passed the BBB was hydrolyzed to [^{11}C]**11** within 5 min after administration. Though the first hydrolysis step should be considered for the quantitative kinetic analysis of PET, the hydrolysis rate of [^{11}C]**5** might be fast enough for the functional analysis of COX imaging in rat brain, because a significant difference

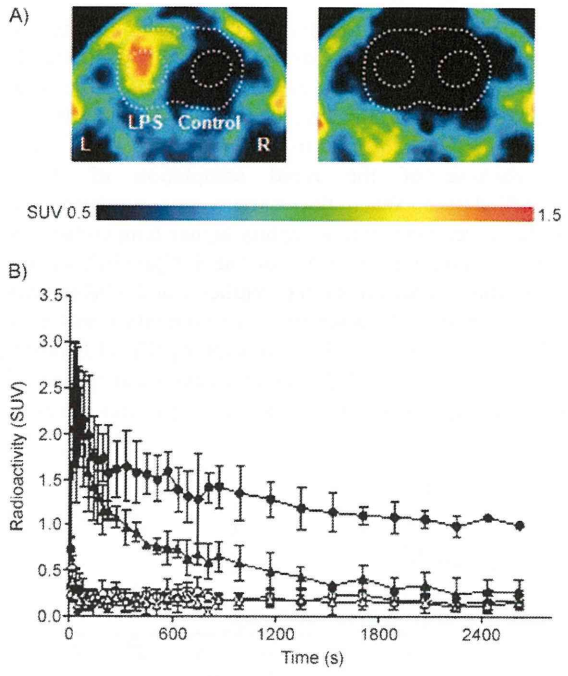

Figure 2. A) Summated PET images (from 5 to 45 min after the tracer injection) of [^{11}C]**5** (left panel) and [^{11}C]**11** (right panel) in rat brain inflammation induced by LPS (50 μg) injection into the left striatum. B) Time–activity curves of [^{11}C]**5** ($n=2$) and [^{11}C]**11** ($n=3$) in the LPS-injected inflammatory area (LPS) and the contralateral region (control). Data are expressed as mean ±SD (●: LPS [^{11}C]**5**, ▲: control [^{11}C]**5**; ○: LPS [^{11}C]**11**, △: control [^{11}C]**11**).

between the inflammatory region and contralateral region was observed in the later time point after the injection (Figure 2B). Thus, [^{11}C]**5** showed appropriate behavior as a proradiotracer for the functional imaging in the rat brain.

Screening study of 2-aryl[^{11}C]propionic acid methyl esters by microPET imaging: To explore the appropriate PET tracers for neuroinflammation, PET studies by using [^{11}C]**1**, [^{11}C]**2**, [^{11}C]**3**, [^{11}C]**4**, [^{11}C]**5**, and [^{11}C]**6** were performed in the rat model of neuroinflammation. PET images with 2-aryl[^{11}C]propionic acid methyl esters demonstrated that all of the proradiotracers, with the exception of [^{11}C]**1**, showed high accumulation in the area of LPS-induced inflammation (Figure 4). Since the radiochemical stability of [^{11}C]**1** was comparable with that of [^{11}C]**2**, the lower brain uptake of [^{11}C]**1** might be derived from the differences of pharmacokinetic properties, such as metabolic stability and/or affinity for efflux pumps at the BBB. Regional brain accumulation of these proradiotracers is shown as a standardized uptake value (SUV) during 40 min (5–45 min post-injection of the tracer) in Table 2. The highest accumulation in the inflammatory area was observed for [^{11}C]**5**, followed by [^{11}C]**6**, [^{11}C]**3**, [^{11}C]**4**, and [^{11}C]**2**, whereas the ratio to the contralateral lesioned area was the highest for [^{11}C]**6** and [^{11}C]**2** (about 4-fold).

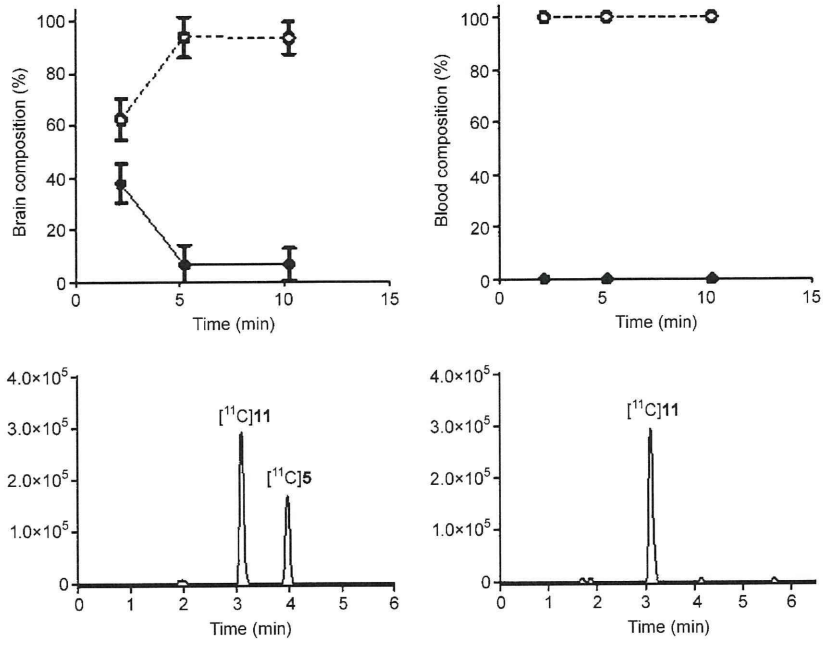

Figure 3. Rat brain (left) and blood (right) compositions of Ketoprofen methyl ester ([^{11}C]**5**, ●) and its pharmacological active metabolite, Ketoprofen ([^{11}C]**11**, ○). Data are expressed as mean ±SD (n=3). Top) Composition of [^{11}C]**5** and [^{11}C]**11**. Bottom) HPLC analyses by radio detector after 2 min.

the ex vivo autoradiography study also revealed the significant reduction of increased radioactivities in the LPS-injected side of the striatum and cortex (Figure 5C). Since many inflammatory-related events, such as organ infiltration and invasion of immune cells, are known to hardly occur in the early phase of inflammation, the incomplete blocking result observed in the inflammatory area may be derived from large amounts of nonspecific accumulation caused by such events.

Currently, PET and related biological studies are being conducted with rodents and nonhuman primates to determine the suitable NSAID PET tracers for in vivo COXs imaging, which is useful for diagnosis and drug development for diseases relating to COXs expression.

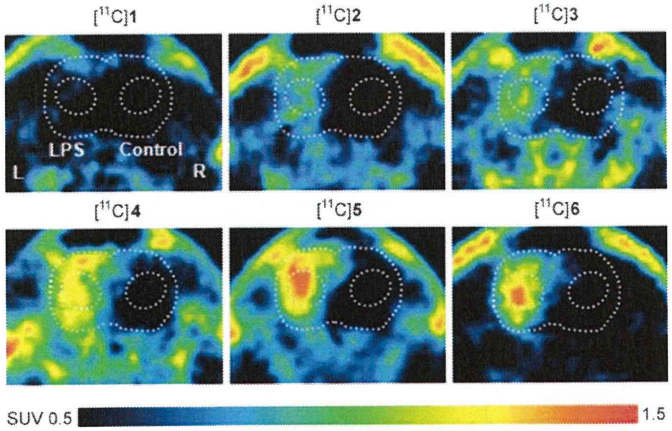

Figure 4. PET images of 2-aryl[^{11}C]propionic acid methyl esters in rat brain inflammation induced by LPS (50 μg) injection into the left striatum.

Table 2. Regional brain accumulation of the 2-aryl[^{11}C]propionic acid methyl esters in the inflammatory area induced by LPS (50 μg) injection into the left striatum.[a]

	SUV LPS injected striatum	contralateral striatum	Ratio LPS/control
[^{11}C]**1**	0.51±0.07	0.30±0.04	1.70±0.24
[^{11}C]**2**	0.92±0.17	0.26±0.02	3.57±0.70
[^{11}C]**3**	0.96±0.03	0.39±0.03	2.50±0.27
[^{11}C]**4**	0.93±0.17	0.39±0.16	2.57±0.63
[^{11}C]**5**	1.21±0.18	0.47±0.12	2.75±1.10
[^{11}C]**6**	1.10±0.18	0.29±0.02	3.76±0.48

[a] The data were expressed as the standardized uptake value (SUV), normalized for injected radioactivity and body weight. SUV=(radioactivity per cubic centimeter tissue/injected radioactivity)×gram body weight. Data are expressed as mean ±SD ([^{11}C]**3** and [^{11}C]**5**, n=2; [^{11}C]**1**, [^{11}C]**2**, [^{11}C]**4**, and [^{11}C]**6**, n=3).

To determine the binding specificity of 2-aryl-[^{11}C]propionic acid methyl esters as proradiotracer in the inflamed area, we performed blocking experiments of [^{11}C]**5** (proradiotracer of [^{11}C]**11**) by using PET and ex vivo autoradiography. Simultaneous injection of authentic Ketoprofen methyl ester (KTP-Me) (10 mg kg^{-1}) with [^{11}C]**5** resulted in a significantly reduced accumulation of radioactivities in the area of LPS-induced inflammation (Figure 5A,B). Images of [^{11}C]**5** (proradiotracer of [^{11}C]**11**) at 50 min post-injection in

Conclusion

To construct a PET tracer library, we developed a method for common and efficient rapid ^{11}C-labeling of 2-arylpropionic acids and their methyl esters through the [^{11}C]carbon–carbon bond formation; this method provided a moderate radiochemical yield with high chemical and radiochemical purity.[25] Although the pharmacologically active forms, 2-aryl[^{11}C]propionic acids, showed low levels of brain uptake, we expect that these compounds will be applied to peripheral imaging. On the other hand, 2-aryl[^{11}C]propionic acid methyl esters showed good brain penetration. In addi-

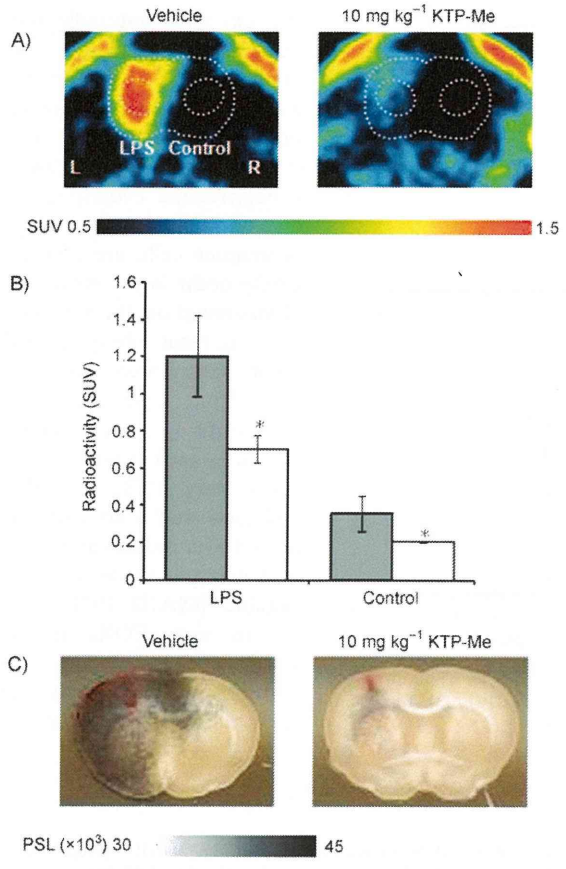

Figure 5. A) PET images of [^{11}C]**5** blocked by excess unlabeled Ketoprofen methyl ester (KTP-Me) in rat brain inflammation induced by LPS (0.5 μg) injection into the left striatum. Unlabeled KTP-Me (10 mg kg^{-1}) was simultaneously administered with radiotracer. B) Accumulated radioactivity of [^{11}C]**5** with simultaneous injection of KTP-Me in the inflamed area (LPS) and the contralateral region (control). The data are expressed as SUV. The results are means ±SD (Vehicle ( ), $n=5$; 10 mg KTP-Me (□), $n=4$). *: $p<0.05$; unpaired t-test. C) Ex vivo autoradiographic images of [^{11}C]**5** at 50 min post-injection. The autoradiographic images coregistered with their brain-slice photographs.

tion, the metabolite analysis of the ester [^{11}C]**5** in the rat brain showed that it was converted into the pharmacologically active form [^{11}C]**11**. The studies of a rat model of LPS-induced brain inflammation showed that [^{11}C]**2**, [^{11}C]**3**, [^{11}C]**4**, [^{11}C]**5**, and [^{11}C]**6** were more highly taken up into the LPS-treated area than the contralateral nontreated area. The blocking study in PET and ex vivo autoradiography revealed the specificity of [^{11}C]**5** (proradiotracer of [^{11}C]**11**) for the target regions.

Experimental Section

Chemistry: All chemicals and solvents were purchased from Sigma–Aldrich Japan (Tokyo, Japan), Wako Pure Chemical Industries (Osaka, Japan), Tokyo Kasei Kogyo (Tokyo, Japan), and Nacalai Tesque (Kyoto, Japan), and were used without further purification. Carbon-11 was produced by an ^{14}N(p,α)^{11}C nuclear reaction by using a CYPRIS HM-12S Cyclotron (Sumitomo Heavy Industry, Tokyo, Japan). An original automated radiolabeling system consisting of the heating of the reaction mixture, dilution, HPLC injection, fractional collection, evaporation, and sterile filtration was used for the production of [^{11}C]CH_3I and the ^{11}C-labeling. Purification with semi-preparative HPLC was performed on a JASCO system (Tokyo, Japan). Radioactivity was quantified with an ATOMLAB^{TM}300 dose calibrator (Aloka, Tokyo, Japan). Analytical HPLC was performed on a Shimadzu system (Kyoto, Japan) equipped with pumps and a UV detector, and the effluent radioactivity was determined by using a RLC700 radio analyzer (Aloka). The columns used for the analytical and semi-preparative HPLC were COSMOSIL $5C_{18}$ MS-II and AR-II (Nacalai Tesque). [^{11}C]CH_3I was prepared as previously described.[26]

Radiosynthesis of [^{11}C]Ibuprofen methyl ester (1): Sodium hydride (1 mg) was added to a solution of methyl (4-isobutylphenyl)acetate in anhydrous DMF (200 μL) under an Ar atmosphere. [^{11}C]CH_3I was transported by a stream of helium (30 mL min^{-1}) and trapped in the mixture at 30 °C for 2 min. After the addition of a solution of 25% ascorbic acid (50 μL), water (400 μL), and acetonitrile (400 μL), the resulting mixture was injected into preparative HPLC (mobile phase: acetonitrile/10 mM ammonium formate 65:35; column: COSMOSIL, $5C_{18}$-MS-II, 10 (i.d.)×250 mm, 5 μm; flow rate: 6 mL min^{-1}; UV detection: 195 nm; retention time: 15 min). The desired fraction was collected into a flask containing 25% ascorbic acid (200 μL) and the organic solvent was removed under reduced pressure. The desired radiotracer was dissolved in a mixture of polysorbate 80, propylene glycol, and saline (0.1:1:10 v/v/v, 4 mL). The total synthesis time including HPLC purification and radiopharmaceutical formulation for intravenous administration was 28 min. The isolated radioactivity was 4.0 GBq at the end of synthesis and the specific radioactivity was 23 GBq μmol^{-1}. The chemical identity of [^{11}C]Ibuprofen methyl ester was confirmed by co-injection with the authentic sample of Ibuprofen methyl ester on analytical HPLC (mobile phase: acetonitrile/water 70:30; column: COSMOSIL, $5C_{18}$-AR-II, 4.6 (i.d.)×150 mm, 5 μm; flow rate: 1 mL min^{-1}; UV detection: 210 nm; retention time: 5.3 min). The chemical purity analyzed at 210 nm and the radiochemical purity were greater than 99%.

Radiosynthesis of [^{11}C]Naproxen methyl ester (2): The radiosynthesis method was similar to that of [^{11}C]Ibuprofen methyl ester (**1**). [^{11}C]Naproxen methyl ester was purified by semi-preparative HPLC (mobile phase: acetonitrile/water=65:35; column: COSMOSIL, $5C_{18}$-MS-II, 20 (i.d.)×250 mm, 5 μm; flow rate: 10 mL min^{-1}; UV detection: 230 nm; retention time: 16 min). The total synthesis time including HPLC purification and radiopharmaceutical formulation for intravenous administration was 32 min. The isolated radioactivity was 2.5 GBq at the end of synthesis, and the specific radioactivity was 37 GBq μmol^{-1}. The chemical identity of [^{11}C]Naproxen methyl ester was confirmed by co-injection with the authentic sample of Naproxen methyl ester on analytical HPLC (mobile phase: acetonitrile/water 65:35; column: COSMOSIL, $5C_{18}$-MS-II, 4.6 (i.d.)×150 mm, 5 μm; flow rate: 1 mL min^{-1}; UV detection: 230 nm; retention time: 5.5 min). The chemical purity analyzed at 230 nm and the radiochemical purity were greater than 99%.

Radiosynthesis of [^{11}C]Flurbiprofen methyl ester (3): The radiosynthesis method was similar to that of [^{11}C]Ibuprofen methyl ester (**1**). [^{11}C]Flurbiprofen methyl ester was purified by semi-preparative HPLC (mobile phase: acetonitrile/water 75:25; column: COSMOSIL, $5C_{18}$-MS-II, 20 (i.d.)×250 mm, 5 μm; flow rate: 10 mL min^{-1}; UV detection: 254 nm; retention time: 15 min). The total synthesis time including HPLC purification and radiopharmaceutical formulation for intravenous administration was 35 min. The isolated radioactivity was 5.8 GBq at the end of synthesis, and the specific radioactivity was 41 GBq μmol^{-1}. The chemical identity of [^{11}C]Flurbiprofen methyl ester was confirmed by co-injection with the authentic sample of Flurbiprofen methyl ester on analytical HPLC (mobile phase: acetonitrile/water 60:40; column: COSMOSIL, $5C_{18}$-AR-II, 4.6 (i.d.)×100 mm, 5 μm; flow rate: 1 mL min^{-1}; UV detection: 254 nm; retention time: 5.9 min). The chemical purity analyzed at 254 nm and the radiochemical purity were greater than 99%.

Radiosynthesis of [^{11}C]Fenoprofen methyl ester (4): The radiosynthesis method was similar to that of [^{11}C]Ibuprofen methyl ester (**1**). [^{11}C]Fenoprofen methyl ester was purified by semi-preparative HPLC (mobile phase: acetonitrile/water 70:30; column: COSMOSIL, 5C_{18}-MS-II, 20 (i.d.)×250 mm, 5 μm; flow rate: 10 mL min^{-1}; UV detection: 206 nm; retention time: 17 min). The total synthesis time including HPLC purification and radiopharmaceutical formulation for intravenous administration was 41 min. The isolated radioactivity was 4.8 GBq at the end of synthesis and the specific radioactivity was 43 GBq μmol^{-1}. The chemical identity of [^{11}C]Fenoprofen methyl ester was confirmed by co-injection with the authentic sample of Fenoprofen methyl ester on analytical HPLC (mobile phase: acetonitrile/water 60:40; column: COSMOSIL, 5C_{18}-AR-II, 4.6 (i.d.)×100 mm, 5 μm; flow rate: 1 mL min^{-1}; UV detection: 220 nm; retention time: 5.8 min). The chemical purity analyzed at 220 nm and the radiochemical purity were greater than 99%.

Radiosynthesis of [^{11}C]Ketoprofen methyl ester (5): The radiosynthesis method was similar to that of [^{11}C]Ibuprofen methyl ester (**1**). [^{11}C]Ketprofen methyl ester was purified by semi-preparative HPLC (mobile phase: acetonitrile/water 70:30; column: COSMOSIL, 5C_{18}-MS-II, 20 (i.d.)×250 mm, 5 μm; flow rate: 10 mL min^{-1}; UV detection: 254 nm; retention time: 12 min). The total synthesis time including HPLC purification and radiopharmaceutical formulation for intravenous administration was 28 min. The isolated radioactivity was 6.1 GBq at the end of synthesis and the specific radioactivity was 63 GBq μmol^{-1}. The chemical identity of [^{11}C]Ketoprofen methyl ester was confirmed by co-injection with the authentic sample of Fenoprofen methyl ester on analytical HPLC (mobile phase: acetonitrile/water 60:40; column: COSMOSIL, 5C_{18}-AR-II, 4.6 (i.d.)×100 mm, 5 μm; flow rate: 1 mL min^{-1}; UV detection: 254 nm; retention time: 5.8 min). The chemical purity analyzed at 254 nm and the radiochemical purity were greater than 99%.

Radiosynthesis of [^{11}C]Loxoprofen methyl ester (6): The radiosynthesis method was similar to that of [^{11}C]Ibuprofen methyl ester (**1**). [^{11}C]Loxoprofen methyl ester was purified by semi-preparative HPLC (mobile phase: acetonitrile/10 mM ammonium formate 50:50; column: COSMOSIL, 5C_{18}-MS-II, 10 (i.d.)×250 mm, 5 μm; flow rate: 6 mL min^{-1}; UV detection: 220 nm; retention time: 10 min). The total synthesis time including HPLC purification and radiopharmaceutical formulation for intravenous administration was 36 min. The isolated radioactivity was 2.2 GBq at the end of synthesis, and the specific radioactivity was 28 GBq μmol^{-1}. The chemical identity of [^{11}C]Loxoprofen methyl ester was confirmed by co-injection with the authentic sample of Loxoprofen methyl ester on analytical HPLC (mobile phase: acetonitrile/water 45:55; column: COSMOSIL, 5C_{18}-MS-II, 4.6 (i.d.)×150 mm, 5 μm; flow rate: 1 mL min^{-1}; UV detection: 220 nm; retention time: 11.6 min). The chemical purity analyzed at 220 nm and the radiochemical purity were greater than 99%.

Radiosynthesis of [^{11}C]Ibuprofen (7): Sodium hydride (1 mg) was added to a stirred solution of methyl (4-isobutylphenyl)acetate in anhydrous DMF (200 μL) under an Ar atmosphere. [^{11}C]CH_3I was transported by a stream of helium (30 mL min^{-1}) and trapped in the mixture at room temperature for 2 min. A total of 300 μL of 2 M sodium hydroxide was added to the reaction mixture, and then it was heated at 50 °C for 1 min. After addition of a solution of 10% formic acid in acetonitrile (300 μL), the mixture was diluted with 50% acetonitrile in water (300 μL). The given reaction mixture was injected into preparative HPLC (mobile phase: acetonitrile/10 mM sodium phosphate buffer (pH 7.4) 34:66; column: COSMOSIL, 5C_{18}-MS-II, 20 (i.d.)×250 mm, 5 μm; flow rate: 10 mL min^{-1}; UV detection: 195 nm; retention time: 16 min). The desired fraction was collected into a flask containing 25% ascorbic acid (200 μL), and the organic solvent was removed under the reduced pressure. The desired radiotracer was dissolved in a mixture of polysorbate 80, propylene glycol, and saline (0.1:1:10 v/v/v, 4 mL). The total synthesis time including HPLC purification and radiopharmaceutical formulation for intravenous administration was 33 min. The isolated radioactivity was 5.0 GBq at the end of synthesis, and the specific radioactivity was 34 GBq μmol^{-1}. The chemical identity of [^{11}C]Ibuprofen was confirmed by co-injection with the authentic sample of Ibuprofen on analytical HPLC (mobile phase: acetonitrile/0.1% phosphoric acid 60:40; column: COSMOSIL, 5C_{18}-MS-II, 4.6 (i.d.)×150 mm, 5 μm; flow rate: 1 mL min^{-1}; UV detection: 210 nm; retention time: 5.8 min). The chemical purity analyzed at 210 nm and the radiochemical purity of [^{11}C]Ibuprofen were greater than 99%.

Radiosynthesis of [^{11}C]Naproxen (8): The radiosynthesis method was similar to that of [^{11}C]Ibuprofen (**7**). [^{11}C]Naproxen was purified by semi-preparative HPLC (mobile phase: acetonitrile/10 mM sodium phosphate buffer (pH 7.4) 22:78; column: COSMOSIL, 5C_{18}-MS-II, 20 (i.d.)×250 mm, 5 μm; flow rate: 10 mL min^{-1}; UV detection: 200 nm; retention time: 19 min). The total synthesis time including HPLC purification and radiopharmaceutical formulation for intravenous administration was 37 min. The isolated radioactivity was 2.7 GBq at the end of synthesis and the specific radioactivity was 30 GBq μmol^{-1}. The chemical identity of [^{11}C]Naproxen was confirmed by co-injection with the authentic sample of Naproxen on analytical HPLC (mobile phase: acetonitrile/1% phosphoric acid 50:50; column: COSMOSIL, 5C_{18}-MS-II, 4.6 (i.d.)×150 mm, 5 μm; flow rate: 1 mL min^{-1}; UV detection: 254 nm; retention time: 5.2 min). The chemical purity analyzed at 254 nm and the radiochemical purity were greater than 99%.

Radiosynthesis of [^{11}C]Flurbiprofen (9): The radiosynthesis method was similar to that of [^{11}C]Ibuprofen (**7**). [^{11}C]Flurbiprofen was purified by semi-preparative HPLC (mobile phase, acetonitrile/10 mM sodium phosphate buffer (pH 7.4) 33:67; column: COSMOSIL, 5C_{18}-MS-II, 20 (i.d.)×250 mm, 5 μm; flow rate: 10 mL min^{-1}; UV detection: 254 nm; retention time: 14 min). The total synthesis time including HPLC purification and radiopharmaceutical formulation for intravenous administration was 40 min. The isolated radioactivity was 3.5 GBq at the end of synthesis and the specific radioactivity was 47 GBq μmol^{-1}. The chemical identity of [^{11}C]Flurbiprofen was confirmed by co-injection with the authentic sample of Flurbiprofen on analytical HPLC (mobile phase: acetonitrile/1% phosphoric acid 50:50; column: COSMOSIL, 5C_{18}-AR-II, 4.6 (i.d.)×100 mm, 5 μm; flow rate: 1 mL min^{-1}; UV detection: 254 nm; retention time: 6.0 min). The chemical purity analyzed at 254 nm and the radiochemical purity were greater than 99%.

Radiosynthesis of [^{11}C]Fenoprofen (10): The radiosynthesis method was similar to that of [^{11}C]Ibuprofen (**7**). [^{11}C]Fenoprofen was purified by semi-preparative HPLC (mobile phase, acetonitrile/10 mM sodium phosphate buffer (pH 7.4) 20:80; column: COSMOSIL, 5C_{18}-MS-II, 20 (i.d.)×250 mm, 5 μm; flow rate: 10 mL min^{-1}; UV detection: 206 nm; retention time: 16 min). The total synthesis time including HPLC purification and radiopharmaceutical formulation for intravenous administration was 40 min. The isolated radioactivity was 6.0 GBq at the end of synthesis and the specific radioactivity was 25 GBq μmol^{-1}. The chemical identity of [^{11}C]Fenoprofen was confirmed by co-injection with the authentic sample of Fenoprofen on analytical HPLC (mobile phase: acetonitrile/0.1% phosphoric acid 45:55; column: COSMOSIL, 5C_{18}-AR-II, 4.6 (i.d.)×100 mm, 5 μm; flow rate: 1 mL min^{-1}; UV detection: 220 nm; retention time: 8.4 min). The chemical purity at 220 nm was more than 98% and the radiochemical purity of [^{11}C]Fenoprofen was greater than 99%.

Radiosynthesis of [^{11}C]Ketoprofen (11): The radiosynthesis method was similar to that of [^{11}C]Ibuprofen (**7**). [^{11}C]Ketoprofen was purified by semi-preparative HPLC (mobile phase: acetonitrile/10 mM sodium phosphate buffer (pH 7.4) 30:70; column: COSMOSIL, 5C_{18}-MS-II, 20 (i.d.)×250 mm, 5 μm; flow rate: 10 mL min^{-1}; UV detection: 254 nm; retention time: 9.7 min). The total synthesis time including HPLC purification and radiopharmaceutical formulation for intravenous administration was 28 min. The isolated radioactivity was 3.8 GBq at the end of synthesis and the specific radioactivity was 40 GBq μmol^{-1}. The chemical identity of [^{11}C]Ketoprofen was confirmed by co-injection with the authentic sample of Ketoprofen on analytical HPLC (mobile phase: acetonitrile/0.1% phosphoric acid 40:60; column: COSMOSIL, 5C_{18}-AR-II, 4.6 (i.d.)×100 mm, 5 μm; flow rate: 1 mL min^{-1}; UV detection: 254 nm; retention time: 6.2 min). The chemical purity at 254 nm and the radiochemical purity were greater than 99%.

Radiosynthesis of [^{11}C]Loxoprofen (12): The radiosynthesis method was similar to that of [^{11}C]Ibuprofen (**7**). [^{11}C]Loxoprofen was purified by semi-preparative HPLC (mobile phase: acetonitrile/10 mM sodium phosphate buffer (pH 7.4) 20:80; column: COSMOSIL, 5C_{18}-MS-II, 20 (i.d.)×

250 mm, 5 μm; flow rate: 10 mL min^{-1}; UV detection: 220 nm; retention time: 16 min). The total synthesis time including HPLC purification and radiopharmaceutical formulation for intravenous administration was 42 min. The isolated radioactivity was 2.0 GBq at the end of synthesis and the specific radioactivity was 28 GBq μmol^{-1}. The chemical identity of [^{11}C]Loxoprofen was confirmed by co-injection with the authentic sample of Loxoprofen on analytical HPLC (mobile phase: acetonitrile/0.1% phosphoric acid 60:40; column: COSMOSIL, 5C$_{18}$-AR-II, 4.6 (i.d.)×100 mm, 5 μm; flow rate: 1 mL min^{-1}; UV detection: 220 nm; retention time: 6.6 min). The chemical purity at 220 nm and the radiochemical purity were greater than 99%.

Experimental animals: The animals were kept in a temperature- and light-controlled environment and had ad libitum access to standard food and tap water. All experimental protocols were approved by the Ethics Committee on Animal Care and Use of the Center for Molecular Imaging Science in RIKEN, and were performed in accordance with the Principles of Laboratory Animal Care (NIH publication no. 85–23, revised 1985).

Generation of neuroinflammation in rats: Male Sprague-Dawley rats (CLEA Japan, Tokyo, Japan) that weighed approximately 300 g received an injection of lipopolysaccharides (LPS) from *Escherichia coli* 026:B6 (Sigma, St. Louis, MO, USA) into the left striatum. Briefly, animals were anesthetized with 50 mg kg^{-1} sodium pentobarbital and stereotaxically injected with LPS into the left striatum with a Hamilton syringe (anterior: +0.2, lateral: +3.2, ventral: −5.5 mm from bregma). Animals were returned to their home cages after the surgery and were housed for 1 day following LPS injection.

PET studies: Rats were anesthetized with a mixture of 1.5% isoflurane and nitrous oxide/oxygen (7:3) and then placed on the PET scanner gantry (microPET Focus 220, Siemens Co., Knoxville, TN, USA). The PET scanner has a spatial resolution of 1.4 mm in FWHM at the center of the field of view at 220 mm in diameter and an axial extent at 78 mm in length. After intravenous bolus injection of 2-aryl[^{11}C]propionic acid or 2-aryl[^{11}C]propionic acid methyl ester (ca. 70 MBq per animal) by means of a venous catheter inserted into the tail vein, a 45 min emission scan was performed. In the blocking experiment, unlabeled compound (10 mg kg^{-1}) was simultaneously injected with radiotracers. Emission data were acquired in list mode, and the data were reconstructed with standard 2D filtered back projection (Ramp filter, cutoff frequency at 0.5 cycles per pixel). Regions of interest (ROI) were placed on the LPS-injected side and the contralateral side of striatum by using image processing software (Pmod ver.3.0, PMOD Technologies Ltd, Zurich, Switzerland) with reference to the rat MRI. Regional uptake of radioactivity in the brain was decay-corrected to the injection time and expressed as the standardized uptake value (SUV), normalized for injected radioactivity and body weight.

Ex vivo autoradiography: Fifty minutes after tracer injection, rats were euthanized and were perfused with saline under deep anesthesia with 1.5% isoflurane. Their brains were quickly removed, and 2 mm thick coronal sections were prepared by using a brain matrix (RBM-2000C, ASI Instruments, Warren, MI, USA) at 4°C. These brain sections were then placed in contact with imaging plates (BAS SR-2040; FUJIFILM, Tokyo, Japan) for 1 h. Autoradiograms were obtained and quantified by using a Bio-Imaging Analyzer System (FLA7000; FUJIFILM). Radioactivity levels in the brain regions were measured and expressed as photostimulated luminescence (PSL)/area [mm^2].

Radioactive metabolite analysis in brain and blood after administration of [^{11}C]5 to normal rats: Male Sprague-Dawley rats weighing around 200 g (n=9) were anesthetized with 1.5% isoflurane before administration of the radiotracers. After intravenous injection of [^{11}C]**5** (ca. 110 MBq per animal) into the rats, blood sampling was performed, and the blood flow was terminated by transection of the abdominal aorta and vein after 2, 5, and 10 min. The brain was removed quickly and subsequently frozen in liquid nitrogen, and then the mixture was homogenized. Two-fold volumes of acetonitrile were added to blood or brain homogenate aliquot, and then the resulting mixture was centrifuged at 12,000 rpm for 2 min at 4°C. The supernatant was evaporated, reconstituted with HPLC mobile phase, and then analyzed for radioactive components by using an HPLC system (Shimadzu Corporation, Kyoto, Japan) with a coupled NaI(Tl) positron detector UG-SCA30 (Universal Giken, Kanagawa, Japan) to measure intact radiotracer and its acid form. A fast-gradient condition created with two switching pumps was used to analyze the samples. An Atlantis T3 column (4.6 (i.d.)×50 mm; Waters, Milford, MA, USA) was used as a reverse-phase analytical column, and a flow rate of 2.0 mL min^{-1} of methanol/water (28:72, v/v) containing 10 mM ammonium acetate (pH 7.2) was the initial condition used. After 0.3 min of the sample injection, the ratio of acetonitrile/water was changed to 80:20 (v/v) linearly for 2.2 min and maintained for the next 2.0 min. The columns were then washed with acetonitrile/water (28:72, v/v) containing 10 mM ammonium acetate (pH 7.2). The elution was monitored by UV absorbance at 254 nm and coupled NaI positron detection. The amount of radioactivity associated with intact radiotracer and its acid form was calculated as a percentage of the total amount of radioactivity.

Acknowledgements

This work was supported in part by a consignment expense for the Molecular Imaging Program on "Research Base for Exploring New Drugs" from the Ministry of Education, Culture, Sports, Science and Technology (MEXT) of Japan. We would like to thank Mr. M. Kurahashi (Sumitomo Heavy Industry Accelerator Service Ltd.) for operating the cyclotron, Ms. K. Tokuda (RIKEN) for supporting rat PET studies, Ms. E. Hayashinaka (RIKEN) for supporting the reconstruction of PET images, and Dr. M. Murai, Mr. K. Noutomi, and Ms.Y. Katayama (RIKEN) for supporting the metabolite analyses.

[1] J. G. Lombardino, *Nonsteroidal Antiinflammatory Drugs*, Wiley, New York, **1985**.
[2] N. V. Chandrasekharan, H. Dai, K. L. T. Roos, N. K. Evanson, J. Tomsik, T. S. Elton, D. L. Simmons, *Proc. Natl. Acad. Sci. USA* **2002**, *99*, 13926–13931.
[3] a) M. E. Phelps *PET: Molecular Imaging and its Biological Applications*, Springer, New York, **2004**; b) J. S. Fowler, A. P. Wolf, *Acc. Chem. Res.* **1997**, *30*, 181–188; c) S. M. Ametamey, *Chem. Rev.* **2008**, *108*, 1501–1516; d) P. W. Miller, N. J. Long, R. Vilar, A. D. Gee, *Angew. Chem.* **2008**, *120*, 9136–9172; *Angew. Chem. Int. Ed.* **2008**, *47*, 8998–9033.
[4] G. Lappin, R. C. Garner, *Nat. Rev. Drug Discovery* **2003**, *2*, 233–240.
[5] M. Bergström, R. J. Hargreaves, H. D. Burns, M. R. Goldberg, D. Sciberras, S. A. Reins, K. J. Petty, M. Ögren, G. Antoni, B. Långström, O. Eskola, M. Scheinin, O. Solin, A. K. Majumdar, M. L. Constanzer, W. P. Battisti, T. E. Bradstreet, C. Gargano, J. Hietala, *Biol. Psychiatry* **2004**, *55*, 1007–1012.
[6] a) M. Suzuki, K. Sumi, H. Koyama, Siqin, T. Hosoya, M. Takashima-Hirano, H. Doi, *Chem. Eur. J.* **2009**, *15*, 12489–12495; b) H. Doi, I. Ban, A. Nonomiya, K. Sumi, C. Kuang, T. Hosoya, H. Tsukada, M. Suzuki, *Chem. Eur. J.* **2009**, *15*, 4165–4171; c) M. Suzuki, H. Doi, M. Björkman, Y. Andersson, B. Långström, Y. Watanabe, R. Noyori, *Chem. Eur. J.* **1997**, *3*, 2039–2042.
[7] a) H. R. Herschman, J. J. Talley, R. DuBois, *Mol. Imaging. Biol.* **2003**, *5*, 286–303; b) E. F. de Vries, *Curr. Pharm. Des.* **2006**, *12*, 3847–3856; c) S. T. Elder, *Diss. Abstr. Int. B* **1991**, *52*, 2566.
[8] E. F. de Vries, A. van Waarde, A. R. Buursma, W. Vaalburg, *J. Nucl. Med.* **2003**, *44*, 1700–1706.
[9] J. Prabhakaran, V. J. Majo, N. R. Simpson, R. L. Van Heertum, J. J. Mann, J. S. D. Kumar, *J. Labelled Compd. Radiopharm.* **2005**, *48*, 887–895.
[10] E. F. de Vries, J. Doorduin, R. A. Dierckx, A. van Waarde, *Nucl. Med. Biol.* **2008**, *35*, 35–42.

[11] V. J. Majo, J. Prabhakaran, N. R. Simpson, R. L. Van Heertum, J. J. Mann, J. S. D. Kumar, *Bioorg. Med. Chem. Lett.* **2005**, *15*, 4268–4271.

[12] M. Tanaka, Y. Fujisaki, K. Kawamura, K. Ishiwata, Qinggeletu, F. Yamamoto, T. Mukai, M. Maeda, *Biol. Pharm. Bull.* **2006**, *29*, 2087–2094.

[13] a) T. J. McCarthy, A. U. Sheriff, M. J. Graneto, J. J. Talley, M. J. Welch, *J. Nucl. Med.* **2002**, *43*, 117–124; b) Y. Fujisaki, K. Kawamura, W. F. Wang, K. Ishiwata, F. Yamamoto, T. Kuwano, M. Ono, M. Maeda, *Ann. Nucl. Med.* **2005**, *19*, 617–625; c) F. R. Wüst, A. Hohne, P. Metz, *Org. Biomol. Chem.* **2005**, *3*, 503–507; d) J. Prabhakaran, M. F. Underwood, R. V. Parsey, V. Arango, V. J. Majo, N. R. Simpson, R. Van Heertum, J. J. Mann, J. S. D. Kumar, *Bioorg. Med. Chem.* **2007**, *15*, 1802–1807; e) F. Wuest, T. Kniess, R. Bergmann, J. Pietzsch, *Bioorg. Med. Chem.* **2008**, *16*, 7662–7670.

[14] a) J. E. Dinchuk, B. D. Car, R. J. Focht, J. J. Johnston, B. D. Jaffee, M. B. Covington, N. R. Contel, V. M. Eng, R. J. Collins, P. M. Czerniak, S. A. Gorry, J. M. Trzaskos, *Nature* **1995**, *378*, 406–409; b) R. Langenbach, C. Loftin, C. Lee, H. Tiano, *Biochem. Pharmacol.* **1999**, *58*, 1237–1246; c) R. Langenbach, S. G. Morham, H. F. Tiano, C. D. Loftin, B. I. Ghanayem, P. C. Chulada, J. F. Mahler, C. A. Lee, E. H. Goulding, K. D. Kluckman, H. S. Kim, O. Smithies, *Cell* **1995**, *83*, 483–492; d) S. G. Morham, R. Langenbach, C. D. Loftin, H. F. Tiano, N. Vouloumanos, J. C. Jennette, J. F. Mahler, K. D. Kluckman, A. Ledford, C. A. Lee, O. Smithies, *Cell* **1995**, *83*, 473–482; e) J. L. Wallace, A. Bak, W. McKnight, S. Asfaha, K. A. Sharkey, W. K. MacNaughton, *Gastroenterology* **1998**, *115*, 101–109.

[15] M. Takashima-Hirano, Y. Cui, T. Takashima, E. Hayashinaka, Y. Wada, Y. Watanabe, H. Doi, M. Suzuki, *J. Labelled Compd. Radiopharm.* **2009**, *52*, S435.

[16] Although the method by using malonic esters as the precursor for the synthesis of 2-[^{11}C][14]methyl-fatty acids was reported, it requires three steps including methylation, hydrolysis, and decarboxylation to give our desired compounds. See reference: K. Ogawa, M. Sasaki, T. Nozaki, *Appl. Radiat. Isot.* **1997**, *48*, 623–630.

[17] a) T. D. Warner, F. Giuliano, I. Vojnovic, A. Bukasa, J. A. Mitchell, J. R. Vane, *Proc. Natl. Acad. Sci. USA* **1999**, *96*, 7563–7568; b) D. Riendeau, M. Salem, A. Styhler, M. Ouellet, J. A. Mancini, C. S. Li, *Bioorg. Med. Chem. Lett.* **2004**, *14*, 1201–1203.

[18] a) H. Fujisawa, T. Fujiwara, Y. Takeuchi, K. Omata, *Chem. Pharm. Bull.* **2005**, *53*, 524–528; b) T. Bruzzese, M. Cambieri, R. Ferrari, Ger. Offen. DE2614306, **1976**; c) J. H. Fried, I. T. Harrison, S. African ZA6707597, **1968**; d) S. S. Adams, J. Bernard, J. S. Nichlolson, A. R. Blancafort, U.S. Patent 3755427, **1973**; e) Y. L. Chen, U.S. Patent 2005032859, **2005**; f) D. E. Bays, R. V. Foster, S.African ZA6804682, **1969**; g) A. Terada, E. Misaka, K. Hasegawa, Fr. Demande FR2483918, **1981**.

[19] a) T. Fukumura, R. Y. Nakao, M. Yamaguchi, K. Suzuki, *Appl. Radiat. Isot.* **2004**, *61*, 1279–1287; b) P. J. H. Scott, B. G. Hockley, H. F. Kung, R. Machanda, W. Zhang, M. R. Kilbourn, *Appl. Radiat. Isot.* **2009**, *67*, 88–94.

[20] All products were isolated as a racemic mixture. Generally, the *S* enantiomer of 2-arylproiponic acid is pharmacologically active in terms of the cyclooxygenase inhibition. However, the majority of 2-arylpropionic acids are prepared in a racemic mixture because an isomerase enzyme (2-arylpropionyl-CoA epimerase) exists in vivo system that converts the inactive *R* enantiomer into the active *S* form, see: a) C. Reichel, R. Brugger, H. Bang, G. Geisslinger, K. Brune, *Mol. Pharmacol.* **1997**, *51*, 576–582; exceptionally, a few inhibitors, such as Flurbiprofen, undergo such a bioconversion to a very little extent in vitro or in vivo systems, see: b) D. D. Leipold, D. Kantoci, E. D. Murray, D. D. Quiggle, W. J. Wechter, *Chirality* **2004**, *16*, 379–387; optical resolution by chiral column chromatography would be effective to separate racemic-2-aryl[^{11}C]propionic acids and esters into the corresponding *R* and *S* enantiomers, respectively, as exemplified by (*R*)-Flurbiprofen (retention time: 10 min) and (*S*)-Flurbiprofen (retention time: 13 min) (mobile phase: 0.05% trifluoroacetic acid in hexane/0.05% trifluoroacetic acid in ethanol 95:5; column: CHIRALPAK AD-H 10 (i.d.) × 250 mm, 5 μm (Daicel Chemical Industries, Tokyo, Japan); flow rate: 6 mL min^{-1}; UV detection: 254 nm). If necessary, the use of an optically active PET tracer will be reported with the detailed resolution method in due course.

[21] H. B. Choi, J. K. Ryu, S. U. Kim, J. G. McLarnon, *J. Neurosci.* **2007**, *27*, 4957–4968.

[22] J. L. Eriksen, S. A. Sagi, T. E. Smith, S. Weggen, P. Das, D. C. McLendon, V. V. Ozols, K. W. Jessing, K. H. Zavitz, E. H. Koo, T. E. Golde, *J. Clin. Invest.* **2003**, *112*, 440–449.

[23] a) O. Inoue, R. Hosoi, S. Momosaki, K. Yamamoto, M. Amitani, M. Yamaguchi, A. Gee, *Nucl. Med. Biol.* **2006**, *33*, 985–989; b) S. Momosaki, R. Hosoi, T. Sanuki, K. Todoroki, M. Yamaguchi, A. Gee, O. Inoue, *Nucl. Med. Biol.* **2007**, *34*, 939–944.

[24] V. W. Pike, *Trends Pharmacol. Sci.* **2009**, *30*, 431–440.

[25] It should be added that this rapid methylation could also be applied to other 2-arylpropionic acid derivatives of NSAIDs, such as, Benoxaprofen, Cycloprofen, Pranoprofen, etc. to form a larger PET tracer library.

[26] B. Långström, G. Antoni, P. Gullberg, C. Halldin, P. Malmborg, K. Nagren, A. Rimland, H. Svard, *J. Nucl. Med.* **1987**, *28*, 1037–1040.

Received: November 5, 2009
Revised: February 4, 2010
Published online: March 10, 2010

Journal of Parkinson's Disease 1 (2011) 395–412
DOI 10.3233/JPD-2011-11070
IOS Press

Survival of Human Induced Pluripotent Stem Cell–Derived Midbrain Dopaminergic Neurons in the Brain of a Primate Model of Parkinson's Disease

Tetsuhiro Kikuchi[a,b,c], Asuka Morizane[a,b], Daisuke Doi[a,b,c], Hirotaka Onoe[d], Takuya Hayashi[b,d], Toshiyuki Kawasaki[d], Hidemoto Saiki[e], Susumu Miyamoto[c] and Jun Takahashi[a,b,c,*]
[a]*Department of Biological Repair, Institute for Frontier Medical Sciences, Kyoto University, Kyoto, Japan*
[b]*Department of Cell Growth and Differentiation, Center for iPS Cell Research and Application, Kyoto University, Kyoto, Japan*
[c]*Department of Neurosurgery, Clinical Neuroscience, Kyoto University Graduate School of Medicine, Kyoto, Japan*
[d]*Functional Probe Research Laboratory, RIKEN Center for Molecular Imaging Science, Kobe, Japan*
[e]*Department of Neurology, Kitano Hospital, Osaka, Japan*

Abstract. Before induced pluripotent stem cells (iPSCs) can be used to treat neurologic diseases, human iPSC-derived neural cells must be analyzed in the primate brain. In fact, although mouse and human iPSCs have been used to generate dopaminergic (DA) neurons that are beneficial in rat models of Parkinson's disease (PD), human iPSC-derived neural progenitor cells (NPCs) have not been examined in primate brains. Here, we generated NPCs at different stages of predifferentiation using a feeder-free culture method, and grafted them into the brains of a monkey PD model and NOD-SCID mice. Magnetic resonance imaging (MRI), positron emission tomography (PET), immunocytochemistry, and behavioral analyses revealed that NPCs pretreated with Sonic hedgehog and fibroblast growth factor-8 followed by glial cell–derived neurotrophic factor, brain-derived neurotrophic factor, ascorbic acid, and dibutyryl cyclic AMP resulted in smaller grafts than those without these treatments, and survived as DA neurons in a monkey brain as long as six months. Thus, for the first time, we describe a feeder-free neural differentiation method from human iPSCs and an evaluation system that can be used to assess monkey PD models.

Keywords: Induced pluripotent stem cells, Parkinson's disease, transplantation, dopaminergic neurons, positron emission tomography

INTRODUCTION

Induced pluripotent stem cells (iPSCs) are a promising avenue for cell replacement therapy in neurologic diseases. For instance, mouse and human iPSCs have been used to generate dopaminergic (DA) neurons that improve symptoms in rat Parkinson's disease (PD) models [1, 2]. For these cells to be used clinically, however, the growth, differentiation, and function of human iPSC-derived neural cells must be evaluated in a primate model. Transplantation of embryonic neural tissues has been shown to relieve parkinsonian symptoms both in animal models and human patients [3–5]. In addition, we and others have transplanted monkey embryonic stem cell–derived neural progenitor cells

*Correspondence to: Jun Takahashi, M.D., Ph.D., Department of Biological Repair, Institute for Frontier Medical Sciences, Kyoto University, 53 Shogoin kawahara-cho, Sakyo-ku, Kyoto 606-8507, Japan. Tel.: 81 75 751 4840; Fax: 81 75 751 4840; E-mail: jbtaka@frontier.kyoto-u.ac.jp.

ISSN 1877-7171/11/$27.50

(NPCs) [6, 7] or human NPCs [8] into the brains of monkey PD models. Human iPSC-derived NPCs have yet to be characterized in a primate brain, however. Furthermore, neuronal differentiation and transplantation methods need to be optimized. In this study, we developed a series of methods to induce human iPSCs to become NPCs using a feeder-free culture method, and grafted NPCs at different stages of predifferentiation into the brain of a monkey PD model. We then examined the growth and DA activity of the grafts using magnetic resonance imaging (MRI), positron emission tomography (PET), immunocytochemistry, and behavioral analyses.

MATERIALS AND METHODS

Human iPSC culture

Human iPSCs (253G4) were maintained as previously described [9]. For passage, feeder cells were detached using CTK dissociation solution (0.25% trypsin, 0.1% collagenase IV, 20% KSR, and 1 mM $CaCl_2$ in PBS). The detached iPSC clumps were broken into smaller pieces (20–30 cells) by gentle pipetting, and split at 1 : 3. The cells were used in experiments between passage 20 and 50.

Induction of NPCs from human iPSCs

Human iPSCs were dissociated into single cells using Accumax (Innovative Cell Technologies) and quickly reaggregated in differentiation medium (9000 cells/150 ml/well) in 96-well low cell-adhesion plates (Lipidure-Coat U96 w; Nunc). Differentiation medium contained DMEM/F12 supplemented with 5% KSR, 2 mM glutamine, 0.1 mM nonessential amino acids, and 0.1 mM 2-mercaptoethanol. For the first three days, 50 μM Y-27632 (Wako) [10, 11], 2 μM dorsomorphin, and 10 μM SB-431542 [12] were added to the culture medium. On day 14, iPSC-derived spheres were replated on 6-cm Petri dishes containing neurobasal medium (Gibco) supplemented with B-27 and 2 mM L-glutamine. For the indicated samples, 200 mg/ml Sonic hedgehog (Shh) and 100 mg/ml fibroblast growth factor (FGF)-8 were added on days 14–28. After day 28, the medium was replaced with neurobasal medium supplemented with B-27, 2 mM L-glutamine, 2 ng/ml glial cell–derived neurotrophic factor (GDNF), 10 ng/ml brain-derived neurotrophic factor (BDNF), 1 mM dibutyryl cyclic AMP (dbcAMP), and 200 nM ascorbic acid.

Quantitative reverse transcription-polymerase chain reactions (RT-PCRs)

Total RNA was extracted using an RNeasy Mini Kit (Qiagen), and reverse transcribed using the Super Script III First-Strand Synthesis System (Invitrogen). Quantitative PCRs were carried out with SYBR Green mix (ABI) and the ABI StepOne Plus RT-PCR system. Data was assessed using a standard curve and normalized based on β-actin expression. Primer sequences are shown in supplementary Table 1.

Immunocytochemistry

In vitro immunohistochemical analyses were carried out after samples were permeabilized and blocked with 0.3% Triton X-100 and 2.5% donkey serum. Spheres were fixed with 4% paraformaldehyde, frozen, and cut with a cryostat (Leica) at 10-μm thickness. Primary antibodies are shown in supplementary Table 2. Appropriate donkey secondary antibodies conjugated with Alexa 488 or Alexa 594 were used. For nuclear staining, 200 ng/ml 4′,6-diamidino-2-phenylindole was added to the final wash. Immunoreactive cells were visualized using a fluorescence microscope (BZ-9000, Keyence) and a confocal laser-scanning microscope (Fluoview FV1000D, Olympus). For quantification, cells in more than three randomly selected 40× fields were counted from at least three independent cultures. In *in vivo* studies, animals were transcardially perfused with 4% paraformaldehyde. The excised brain was frozen, cut with a microtome at 40-μm thickness, and stained as free-floating sections. In mice, tyrosine hydroxylase $(TH)^+$ cells and $Ki67^+$ cells were counted among 3.0×10^3 cells in at least five 40× fields for each graft. In the monkey, TH^+ cells were counted in every ninth section throughout the graft using BZ Analyzer II (Keyence), whereas $Ki67^+$ cells were counted in at least three 40×fields for one tract and 3.0×10^4 cells were examined in each graft. Hematoxylin–eosin (H–E) staining was performed according to standard procedures.

Animals and cell transplantation

An adult male cynomolgus monkey (*Macaca fascicularis*; 3 years old) weighing 2.63 kg was obtained from Shin Nippon Biomedical Laboratories (Kagoshima, Japan). The monkey and mice were cared for and handled according to the Guidelines for Animal Experiments of Kyoto University and the Guide for the Care and Use of Laboratory Animals of the Institute

of Laboratory Animal Resources (Washington, DC, USA). To create a parkinsonian model, the monkey was injected intravenously with 1-methyl-4-phenyl-1,2,3,6-tetrahydropyridine (MPTP) HCl (0.4 mg/kg as a free base; Sigma–Aldrich) twice a week until we observed persistent parkinsonian symptoms, such as tremor, bradykinesia, and impaired balance. Stable parkinsonian symptoms were observed for more than 12 weeks before the animal was used for the experiments. The coordinates of the targets were obtained using MRI, and human iPSC-derived NPCs were stereotactically transplanted into the bilateral putamen of the MPTP-treated monkey (d28 spheres on the right side, d42 spheres on the left side). The sphere suspension was prepared at 1×10^5 cells/μl, and 1 μl of this suspension was injected along six tracts on each side (four injection sites/tract; 4.8×10^6 cells/animal). After surgery, the monkey was given antibiotics for three days and a daily intravenous immunosuppressant (FK506, 0.05 mg/kg; Astellas Pharma) until sacrifice. Average trough values of circulating FK506 were 14.0 ng/ml ($n = 3$). Five-week-old male NOD/ShiJic-scid/Jcl mice (CLEA Japan) were also used as transplant recipients. Using a 26-gauge needle, each mouse received a stereotactic injection of 1 μl of cell solution (253G4-derived cells: 1×10^5 cells/μl) in the right side of the striatum (from the Bregma: A +0.5, L +1.8, V +3.0, incisor bar 0). Six months after transplantation, the animals were sacrificed and analyzed.

MRI

T1- and T2-weighted images were obtained using a 3-Tesla MRI scanner (Siemens Healthcare) and an 8-channel receiving coil (see Supplementary Methods for details of the MRI scans). Graft volume was analyzed using Functional Magnetic Resonance Images of Brain (FMRIB) Software Libraries [13]. In T1- and T2-weighted images, nonbrain structures were removed using the Brain Extraction Tool [14] and were coregistered with each other based on rigid body transformation using FMRIB's Linear Registration Tool [15]. Next, to identify the graft region, we subjected T1- and T2-weighted images to automated segmentation using the Fast Automated Segmentation Tool [16], which is based on a hidden Markov random field model and an associated expectation–maximization algorithm. We segmented and searched a multichannel set of T1- and T2-weighted images of different tissue types. This process reproducibly identified white matter, gray matter, cerebrospinal fluid (CSF) space (plus graft region, if any), and putamen. Next, partial volume images for the CSF plus graft were thresholded at 30%, binarized, and manually edited to remove the CSF region. The resulting segment image of the graft was used to calculate the graft volume.

PET

A bolus of 6-[^{18}F]fluoro-L-3,4-dihydroxyphenylalanine ([^{18}F]DOPA), [^{11}C]dihydrotetrabenazine ([^{11}C]DTBZ), (*E*)-*N*-(3-iodoprop-2-enyl)-2β-carbo [^{11}C]methoxy-3β-(4-methylphenyl)nortropane ([^{11}C] PE2I), or 3′-deoxy-3′-[^{18}F]fluorothymidine ([^{18}F] FLT) (37 MBq/kg in 2.0 ml of saline) was intravenously delivered within 10 sec under anesthesia via continuous infusion of propofol (10–20 mg/kg/hr). For [^{18}F]DOPA PET scans, a solution of carbidopa (10 mg/kg) was administered intravenously 5 min prior to the scan to minimize peripheral decarboxylation of [^{18}F]DOPA. PET images were acquired using a microPET Focus-220 system (Siemens Healthcare) with a scan duration of 90 min in three-dimensional list mode (see Supplementary Methods for preparation steps and image analysis). The axial and transaxial resolutions of the PET scanner were 1.35 mm at full-width half-maximum. Transmission scanning was performed for 30 min with a rotating 68Ge-68Ga pin source (18.5 MBq) to determine the attenuation factor for image reconstruction just before an emission scan. PET images of [^{18}F]FLT summed over 60 min (30–90 min after the injection) were converted into standardized uptake values and used for further imaging analysis. To determine anatomic locations, PET images were coregistered onto magnetic resonance images using a three-dimensional rigid-body alignment program from image analysis software (PMOD).

Behavioral analysis

The behavior of the monkey was evaluated according to a previously described rating scale for monkey PD models [6]. The normal and minimum score is 0, whereas the maximum total score is 24. The evaluation was performed by a trained examiner who was not involved in the cell transplantation procedure. Spontaneous movements were measured as previously described [17]. Video records were analyzed using the Vigie Primates video-based analysis system (View Point, Lyon, France), and changes in pixels from one image to the next were counted every 66.67 ms. Movements were categorized into one of three levels

based on the number of pixel changes per 66.67 ms (large: more than 501 pixels; medium: 101 to 500 pixels; small: less than 100 pixels). The total time spent making each type of movement was then determined. During the raisin pick-up test, the monkey was placed in a special cage with a small slit through which it could pick up a raisin placed 20 cm from the cage. During a single session, the monkey reached for 20–24 raisins (10–12 raisins on each side).

Dopamine release assay

Accutase (Innovative Cell Technologies) was used to dissociate d28 spheres into small pieces, which were cultured on poly-L-ornithine/laminin–coated culture dishes with neurobasal/B-27 media containing BDNF, GDNF, dbcAMP, and ascorbic acid. Fourteen days later, cells were washed twice with low-concentration KCl solution (20 mM HEPES-NaOH at pH 7.4, 140 mM NaCl, 4.7 mM KCl, 2.5 mM $CaCl_2$, 1.2 mM $MgSO_4$, 1.2 mM KH_2PO_4, and 11 mM glucose) and incubated in the low-concentration KCl solution for 2 min. The medium was subsequently replaced with 1 ml of high-concentration KCl solution (20 mM HEPES-NaOH at pH 7.4, 85 mM NaCl, 60 mM KCl, 2.5 mM $CaCl_2$, 1.2 mM $MgSO_4$, 1.2 mM KH_2PO_4, and 11 mM glucose) and the samples were incubated for 15 min. The solution was then collected and the dopamine concentration was determined using high-performance liquid chromatography (HPLC), including a reverse-phase column and an electrochemical detector system (HTEC-500, Eicom, Japan). Data were obtained from three independent experiments.

Flow cytometry

Cells were harvested on day 14 using Accumax, gently dissociated into single-cell suspensions, and resuspended in phenol-free HBSS (Gibco) containing 1% bovine serum albumin and 0.03% NaN_3. Samples were filtered through cell strainer caps (35-μm mesh; BD Biosciences) and subjected to surface marker staining using anti-PSA-NCAM antibodies (Chemicon). Primary antibodies were added, the samples were incubated at 4°C for 30 min, and the cells were washed twice with HBSS buffer. Secondary antibodies were then added and the samples were incubated at 4°C for 30 min. Dead cells and debris were excluded based on 7-AAD staining. Analyses were performed using a FACSAriaII cell sorter and FACSDiva software (BD Biosciences).

Statistical analysis

Statistical analyses were performed using a commercially available software package (GraphPad Prism, GraphPad Software). Data were analyzed using one-factor ANOVA and Tukey's post-hoc analysis, except for the raisin pick-up test (Fig. 6E; Student's *t*-tests). Differences were considered statistically significant when $P<0.05$ ($^{*}P<0.05$, $^{**}P<0.01$, or $^{***}P<0.001$).

RESULTS

Neural differentiation from human iPSCs using serum-free floating cultures

To generate NPCs, we cultured human iPSCs (253G4) [9] as floating spheres in serum-free medium, such that the cell suspension (9000 cells/well) formed one sphere in each well (Fig. 1A). On day 7, the spheres contained primarily $Pax6^+$ neuroepithelial cells (Fig. 1B) and a small number of $Oct3/4^+$ cells (Fig. 1C). On day 14, almost all cells were immunopositive for both Nestin and Pax6 (Fig. 1D), whereas a small population expressed Tuj1 (Fig. 1E) and no $Oct3/4^+$ or $Nanog^+$ cells were observed (data not shown). Furthermore, flow cytometric analysis on day 14 detected the neural cell surface marker PSA-NCAM on $99.8 \pm 0.1\%$ of the cells (Fig. 1F), indicating that the cells were committed to a neural lineage. We then replaced the culture medium with neurobasal medium, and continued the floating culture in the presence or absence of Shh and FGF8. After a 2-week expansion period (days 14–28), immunocytochemistry revealed that most of the cells were $Tuj1^+$ and $3.14 \pm 1.38\%$ of them were TH^+ on day 28 (Fig. 1G, H, K). Next, we removed Shh and FGF8, and added BDNF, GDNF, ascorbic acid, and dbcAMP to promote maturation of DA neurons. After another 2-week expansion period (days 28–42), the percentage of TH^+ DA neurons among the $Tuj1^+$ neurons in the spheres increased to $85.46 \pm 3.13\%$ (Fig. 1I–K). Quantitative RT-PCR analyses revealed that expression of undifferentiated cell markers (Oct3/4, Nanog) decreased, whereas expression of neural cell markers (Sox1, Pax6) markedly increased between days 0 and 14 (Fig. 1L; supplementary Figure 1). Between days 14 and 42, expression levels of TH gradually increased, indicating that the cells moved to a DA fate. Together with neural differentiation, expression levels of introduced genes (Sox2, Klf4) increased slightly, whereas c-Myc expression did not markedly change (supplementary Figure 1). Based

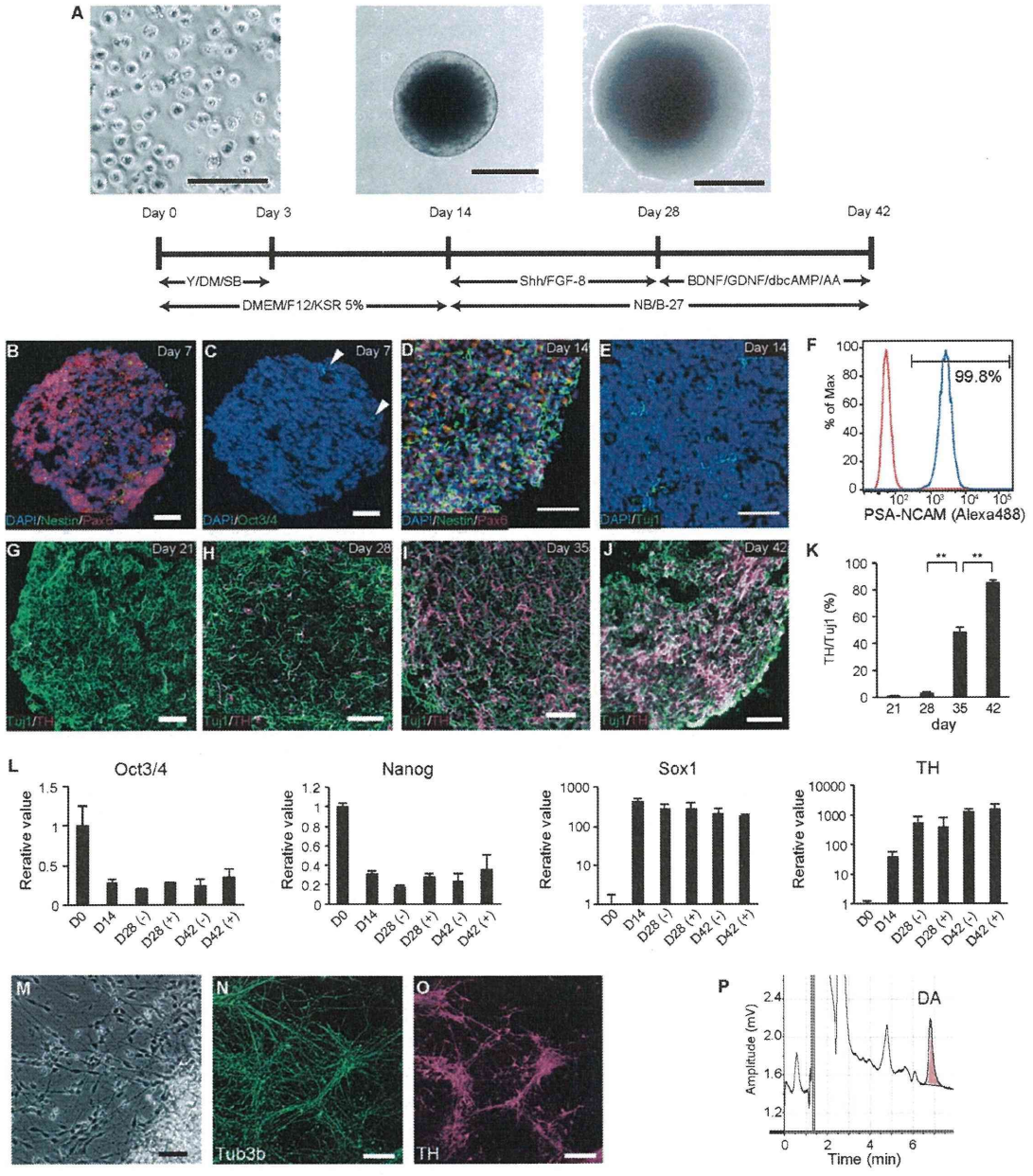

Fig. 1. Neural differentiation using human iPSCs in floating culture. (A) Protocol for the feeder-free floating culture with phase-contrast images of the cells or spheres on days 0, 14, and 28. (B–E) Double- or triple-immunolabeled d7 spheres (B and C) or d14 spheres (D and E). In B and D, Nestin and Pax6 labeling is shown in green and magenta, respectively. In C, Oct3/4 labeling is represented by green, whereas Tuj1 labeling is denoted in green in E. Scale bars, 100 μm. (F) Fluorescence-activated cell sorting analysis of the expression of the neural cell marker PSA-NCAM on day 14. The red line denotes the negative control samples. (G–J) Double-immunolabeled spheres on days 21 (G), 28 (H), 35 (I), and 42 (J). Tuj1 labeling and TH labeling are shown in green and magenta, respectively. Scale bars, 50 μm. (K) Percentages of TH^+ cells among the $Tuj1^+$ cells. Data are presented as means ± SEM (**$P < 0.001$, ANOVA). (L) Time-course analysis of pluripotent cell ($Oct3/4^+$, $Nanog^+$), NPC ($Sox1^+$), and DA neuron (TH^+) markers using quantitative RT-PCRs. Expression levels in iPSCs before differentiation (D0) were set to 1, and the relative expression levels are presented as means ± SEM. Samples were incubated with (+) or without (–) Shh and FGF8 between day 14 and day 28. (M) Phase-contrast and (N, O) immunofluorescence images of differentiated iPSCs on poly-L-ornithine/laminin–coated slides. Scale bars, 50 μm. (P) HPLC analysis showing dopamine release in culture medium containing differentiated iPSCs following KCl-evoked depolarization.

on these results, we compared spheres obtained on day 28 (d28 spheres) and day 42 (d42 spheres) in *in vivo* experiments.

To assess the development of the human iPSC-derived NPCs in our neural differentiation system, we induced DA maturation by culturing d28 spheres on poly-L-ornithine/laminin–coated slides in the presence of BDNF, GDNF, ascorbic acid, and dbcAMP. Two weeks later, the cells extended Tuj1$^+$ neurites and most cells were TH$^+$ (Fig. 1M–O). In addition, HPLC revealed that the cells secreted dopamine into the culture medium in response to high potassium concentrations (196 ± 138 pg/ml; Fig. 1P). Thus, our system produced functional DA neurons from human iPSCs without feeder cells.

Graft growth in NOD-SCID mice

We then compared growth and DA cell differentiation in d28 and d42 spheres in the brains of NOD-SCID mice. Spheres with or without Shh and FGF8 treatment (days 14–28; Fig. 1A) were grafted into the right striatum, and the animals were subjected to immunohistologic studies at 6 months. Grafts derived from d28 spheres (d28 grafts) were significantly larger than d42 grafts (Fig. 2A, B, E). iPSC-derived TH$^+$ cells were observed in these grafts, which also expressed the midbrain DA neuron marker Nurr1 (Fig. 2C, D). Significantly more TH$^+$ cells were observed in d28 grafts without Shh and FGF8 treatment than in d42 grafts with Shh and FGF8 treatment (Fig. 2F), although no significant differences were noted for TH$^+$ cell density in the grafts (Fig. 2G).

Graft growth in an MPTP-treated monkey

We grafted d28 and d42 spheres into the right and left putamina, respectively, of an MPTP-treated cynomolgus monkey (Fig. 3A). Six months after transplantation, MRI showed that grafted cells survived and proliferated in the monkey brain (Fig. 3B). Because MRI of the grafts matched results obtained from H–E staining of brain slices (supplementary Figure 2), we used MRI to measure graft sizes in each tract (Fig. 3C, supplementary Figure 3). For d28 grafts, cells treated with Shh and FGF8 resulted in significantly larger grafts ($172.25 \pm 3.07\,mm^3$, $P < 0.001$) than those obtained with untreated d28(–) cells ($39.21 \pm 6.18\,mm^3$). In contrast, d42 grafts were significantly smaller than d28(+) grafts, and did not significantly differ based on Shh and FGF8 treatment ($19.36 \pm 8.28\,mm^3$ and $22.79 \pm 9.72\,mm^3$ with and without Shh and FGF8, respectively). Between 3 and 6 months, the average doubling times of the d28 grafts with and without Shh and FGF8 were 101 days and 257 days, respectively, whereas those of the d42 grafts were 271 days (the L4 graft was omitted because it stopped expanding) and 148 days, respectively (supplementary Figure 3). In each case, the doubling time between 3 and 6 months post-transplantation was longer than that observed between 1 and 3 months, indicating that the grafts were expanding more slowly. PET with [^{18}F]FLT—a fluorinated thymidine analog—has been previously used to evaluate cell proliferation, for example, in the diagnosis of malignant brain tumors [18]. In this study, however, focal uptake of [^{18}F]FLT was not observed in the 6 months after transplantation (Fig. 3D), and standard uptake values in representative grafts ranged between 0.04 and 0.11 (Fig. 3E). Based on an average standard uptake value of 0.12 in the preoperative monkey, these values were relatively low.

H–E staining showed more cell accumulation in d28 grafts (Fig. 4A) than in d42 grafts (Fig. 4D). In addition, immunohistochemical analyses revealed more Vimentin$^+$ cells and fewer Nestin$^+$ cells in d28 grafts (Fig. 4B, C) than in d42 grafts (Fig. 4E, F). Interestingly, these immature cells were located in the graft core. The percentage of cells expressing Ki67, a marker of proliferating cells, was significantly higher in d28 grafts than in d42 grafts ($0.84 \pm 0.02\%$ vs. $0.23 \pm 0.13\%$; Fig. 4G). Ki67$^+$ cells in d28 grafts were also immunopositive for Vimentin (Fig. 4I), indicating that immature neural or mesenchymal cells were proliferating. In contrast, Ki67$^+$ cells in the d42 grafts were also Nestin$^+$ (Fig. 4H), indicating that some of the grafted cells were still NPCs and a few were proliferating.

DA activity in grafts in an MPTP-treated monkey

Next, we examined *in vivo* differentiation of the grafted cells. TH$^+$ cells were located in the periphery of each graft (Fig. 5A, B), and the density of TH$^+$ cells was higher in d42 grafts treated with Shh and FGF8 (Fig. 5C, D; supplementary Figure 4). The total number of TH$^+$ cells was 3.07×10^4 and 1.26×10^5 in right and left side, respectively (Fig. 5C, supplementary Figure 4). These TH$^+$ cells also expressed markers for mature midbrain DA neurons, including Nurr1, VMAT2, DAT, Girk2, and Pitx3 (Fig. 5E–I). The results suggest that d42 spheres treated with Shh and FGF8 efficiently generated midbrain DA neurons in the monkey brain. Dopamine synthesis, vesicle transport, and dopamine reuptake can be visualized in PET studies using [^{18}F]DOPA, [^{11}C]DTBZ, and [^{11}C]PE2I,

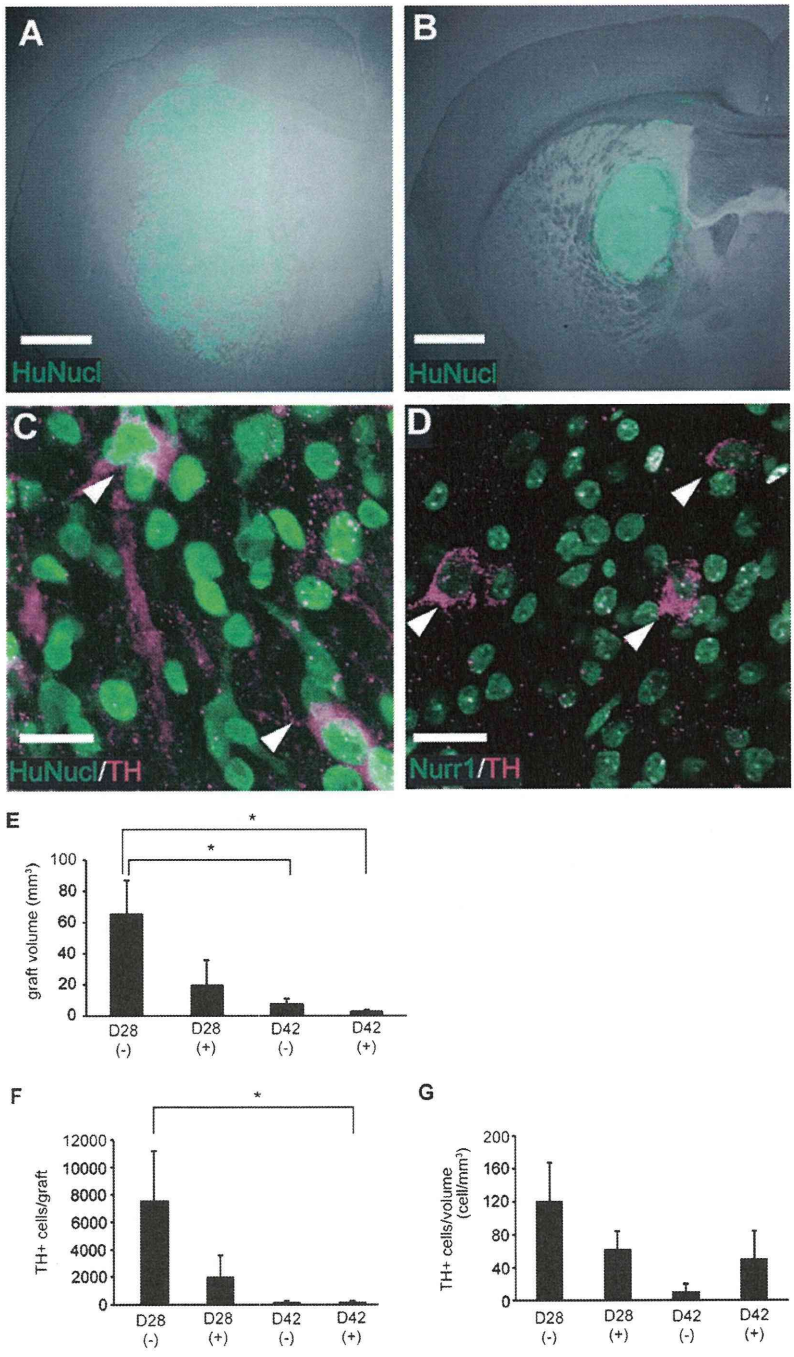

Fig. 2. Growth and differentiation of human iPSC-derived NPCs in mouse brains. (A, B) Representative immunofluorescence images of d28 (A) and d42 (B) grafts with Shh and FGF8 treatment. Human nuclei are labeled green. Scale bars, 1 mm. (C, D) Representative TH^+ cells (red) in these grafts, expressing a human nucleus-specific antigen (green in C) or the midbrain DA neuron marker Nurr1 (green in D). Scale bars, 20 μm. (E–G) Graft volume (E), number of TH^+ cells/graft (F), and number of TH^+ cells/mm^3 (G) in each condition are presented as means ± SEM (*$P < 0.05$, ANOVA; $n = 4$ and 7 for d28 grafts, 5 and 6 for d42 grafts with (+) or without (−) Shh and FGF8 treatment, respectively). All mice were sacrificed and analyzed at 6 months after transplantation.

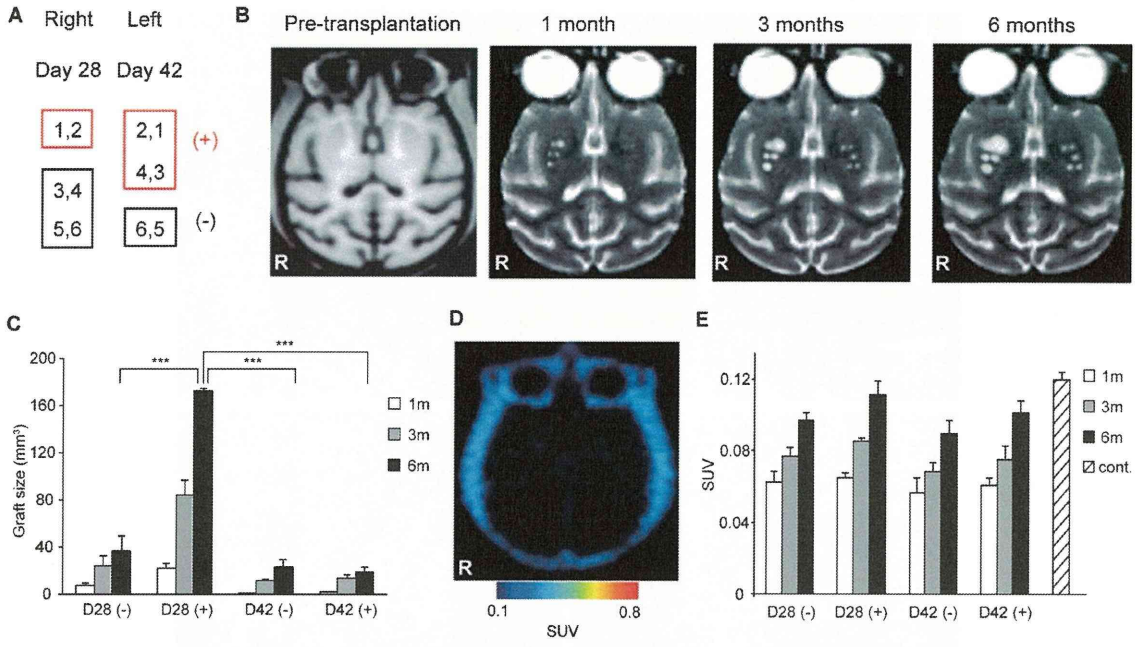

Fig. 3. Growth of NPCs in a MPTP-treated monkey brain. (A) Schematic of the positions of the grafted cells with (+) or without (−) Shh and FGF8 treatment. (B) Axial magnetic resonance images of the monkey before and 1, 3, and 6 months after transplantation. (C) Graft volumes at 1, 3, and 6 months are presented as means ± SEM (***$P < 0.001$, ANOVA). (D) A [^{18}F]FLT-PET image obtained at 6 months after transplantation. (E) Standard uptake values obtained with [^{18}F]FLT-PET at 1, 3, and 6 months after transplantation are presented as means ± SEM. The striped bar represents the average value from preoperative controls ($n = 3$).

respectively [19, 20]. [^{18}F]DOPA-PET at 6 months after transplantation revealed higher Ki values in the d28 grafts, especially those treated with Shh and FGF8 (Fig. 5J, M). This, however, may be a false-positive result owing to detection of 3-O-methyl-6-[^{18}F]fluoro-L-DOPA (OMFD; see discussion). In [^{11}C]DTBZ-PET and [^{11}C]PE2I-PET, ligand binding in the anterior putamen was relatively low (Fig. 5K, L). This finding in the MPTP-treated monkey mirrors the pathology of PD in humans, which is initially characterized by impaired posterodorsal innervations [20]. Intriguingly, the binding potential of [^{11}C]PE2I increased after cell transplantation in d42(+) grafts, suggesting DA cell differentiation from the grafted NPCs (Fig. 5L, M).

Finally, we evaluated the behaviors of the MPTP-treated monkey before and after NPC transplantation. We employed a previously described behavioral rating scale [6], and observed a slight improvement 6 months after transplantation (Fig. 6A). We also performed video-based analysis [17] of spontaneous movements by the monkey. The percentages of time spent making large- and medium-sized movements before transplantation were 0.8% and 7.1%, respectively. Six months later, the time spent making these types of movement increased to 1.0% and 8.9%, respectively (Fig. 6B). The total amount of movement—measured based on changes in video pixels during a 30-min period—also increased after transplantation (898,690 to 995,642 affected pixels; Fig. 6C, D). To distinguish between the effects in the right and left hemispheres, we performed a video-based analysis of the monkey picking up a raisin. We measured the duration of time spent reaching, grasping, and retracting with each arm (supplementary Figure 5). After 6 months, the monkey grasped the raisin and retracted the right arm more quickly (Fig. 6E). Although we did not detect a statistically significant difference, the observed results may reflect more surviving DA neurons in the left striatum.

DISCUSSION

In this study, we used NOD-SCID mice and an MPTP-treated monkey to characterize transplanted human iPSC-derived NPCs. Our results show that human iPSCs incubated in feeder-free floating culture generated functional midbrain DA neurons. Moreover, only NPCs pretreated with Shh and FGF-8 followed by

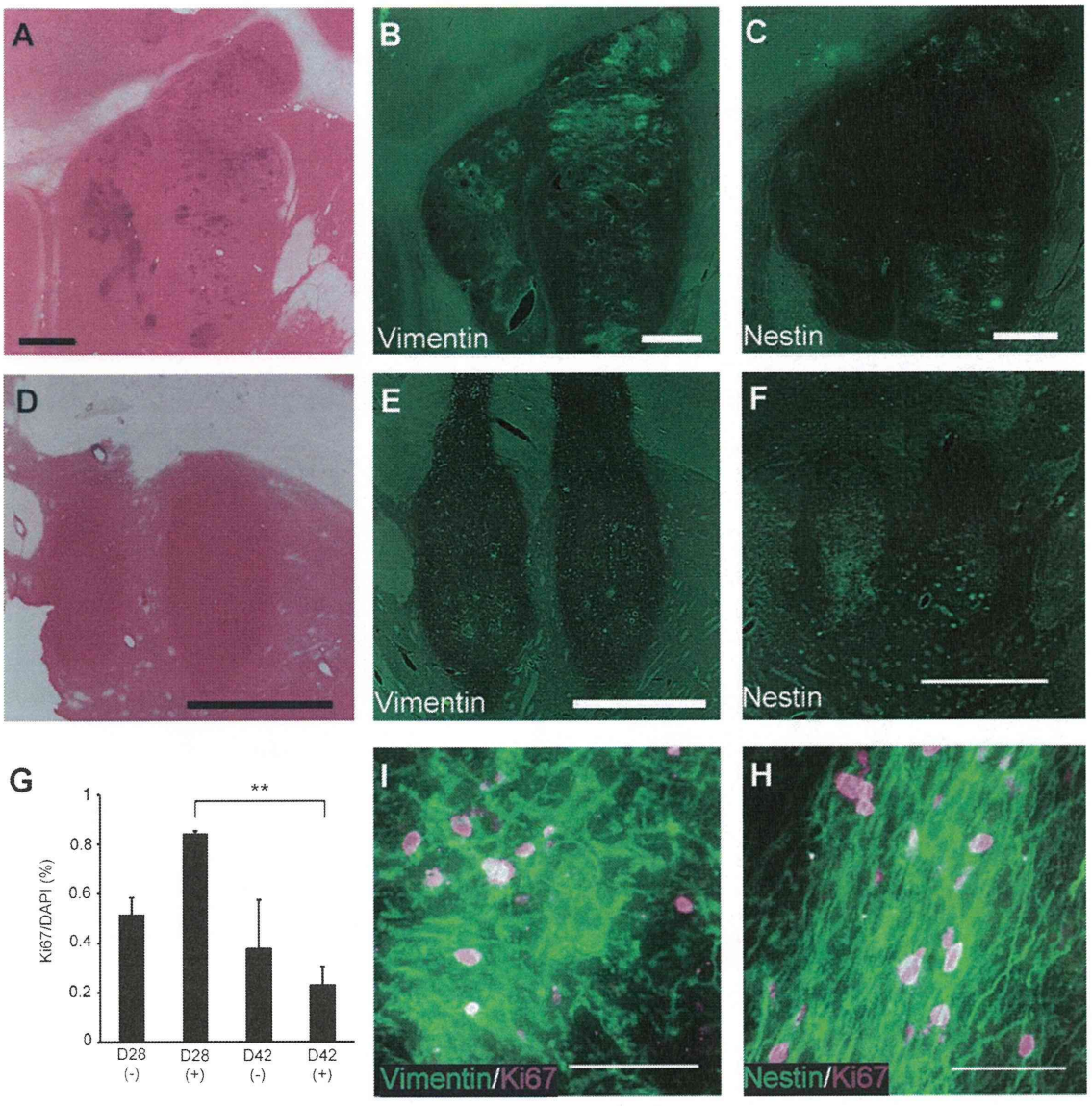

Fig. 4. Expression of immature cell markers in the grafts. (A) H–E staining and (B, C) immunofluorescence images of d28 grafts. Scale bars, 2 mm. (D) H–E staining and (E, F) immunofluorescence images of d42 grafts. Scale bars, 2 mm. (G) Percentages of $Ki67^+$ cells among total cells are presented as means ± SEM (**$P < 0.01$, ANOVA). (I, H) Immunofluorescence images showing labeling of Ki67 (magenta) and Vimentin (green in I) or Nestin (green in H). Scale bars, 50 μm.

GDNF, BDNF, ascorbic acid, and dbcAMP resulted in a substantial number of functional DA neurons in the monkey's brain. Finally, MRI and PET allowed real-time monitoring of *in vivo* cell proliferation and activity.

In two recent studies, midbrain DA neurons were induced to develop from human iPSCs, but the method required coculture with mouse stromal feeder cells [1, 2]. Our feeder-free differentiation method would be more suitable if the cells are to be used clinically. Our mouse and monkey studies demonstrated that d28 spheres resulted in larger grafts at 6 months, suggesting that some NPCs remained immature and proliferated in the brain. These results were consistent with a previous study showing that human embryonic stems cells that differentiated into neurons on PA6 stromal feeder